

# A practical guide to adaptive light-sheet microscopy

Loïc A. Royer<sup>1,3\*</sup>, William C. Lemon<sup>2,3</sup>, Raghav K. Chhetri<sup>2,3</sup>, Philipp J. Keller<sup>1,2\*</sup>

We describe the implementation and use of an adaptive imaging framework for optimizing spatial resolution and signal strength in a light-sheet microscope. The framework, termed AutoPilot, comprises hardware and software modules for automatically measuring and compensating for mismatches between light-sheet and detection focal planes in living specimens. Our protocol enables researchers to introduce adaptive imaging capabilities in an existing light-sheet microscope or use our SiMView microscope blueprint to set up a new adaptive multiview light-sheet microscope. The protocol describes (i) the mechano-optical implementation of the adaptive imaging hardware, including technical drawings for all custom microscope components; (ii) the algorithms and software library for automated adaptive imaging, including the pseudocode and annotated source code for all software modules; and (iii) the execution of adaptive imaging experiments, as well as the configuration and practical use of the AutoPilot framework. Setup of the adaptive imaging hardware and software takes 1–2 weeks each. Previous experience with light-sheet microscopy and some familiarity with software engineering and building of optical instruments are recommended. Successful implementation of the protocol recovers near diffraction-limited performance in many parts of typical multicellular organisms studied with light-sheet microscopy, such as fruit fly and zebrafish embryos, for which resolution and signal strength are improved two- to fivefold.

## Introduction

Light-sheet microscopy is a powerful method for live imaging of biological specimens at high spatiotemporal resolution<sup>1–4</sup>. The high speed and low phototoxicity of this technique make it particularly suitable for imaging developmental and functional processes in large multicellular organisms, such as cell dynamics in entire developing nematode, fruit fly and zebrafish embryos<sup>5–12</sup> or neuronal activity in entire brains of larval fruit flies and zebrafish during behavior<sup>13–17</sup>.

Image formation in a light-sheet microscope relies on selectively illuminating the specimen in a single plane with a laser light sheet formed by lenses or laser scanning<sup>5,18–20</sup> and detecting the fluorescence emitted by fluorophores within this plane with a camera-based, wide-field detection system. Thus, achieving optimal image quality and resolution in a light-sheet microscope requires a good spatial overlap of the illuminating light sheet and the focal plane of the detection system. However, the spatially and temporally variable optical properties of living organisms (and of their surroundings, depending on sample preparation requirements) often introduce large perturbations of the position and orientation of light sheets and detection focal planes inside the specimen. To counteract the degradation in image quality arising from optical perturbations, we developed the AutoPilot framework, which consists of hardware and software components that enable the measurement and minimization of spatial mismatches between light sheets and detection focal planes as a function of space and time in a conventional light-sheet microscope<sup>21</sup>. We previously demonstrated that the use of this adaptive imaging strategy improves spatial resolution and signal strength by a factor of 2–5 in long-term imaging of developing fruit fly and zebrafish embryos and high-speed functional imaging of neuronal activity in the brains of larval zebrafish.

In this protocol, we provide a detailed technical description of all components of the AutoPilot framework, a procedure for integrating adaptive imaging capabilities into a light-sheet microscope and a practical guide to using an AutoPilot-enhanced light-sheet microscope for developmental and functional imaging experiments.

<sup>1</sup>Chan Zuckerberg Biohub, San Francisco, CA, USA. <sup>2</sup>Howard Hughes Medical Institute, Janelia Research Campus, Ashburn, VA, USA. <sup>3</sup>These authors contributed equally: Loïc A. Royer, William C. Lemon, and Raghav K. Chhetri. \*e-mail: [loic.royer@czbiohub.org](mailto:loic.royer@czbiohub.org); [kellerp@janelia.hhmi.org](mailto:kellerp@janelia.hhmi.org)

### Overview of the procedure

We present detailed protocols describing (i) the implementation and mechano-optical degrees of freedom (DOFs) of an adaptive light-sheet microscope based on the AutoPilot framework (Steps 1–21), (ii) the procedure for incorporating AutoPilot hardware modules into an existing light-sheet microscope (Steps 22–29), (iii) the procedure for integrating the core AutoPilot algorithms into the microscope control software of an existing light-sheet microscope (with support for Java, C++ and LabVIEW; Steps 30–34), (iv) the software components of the AutoPilot framework, including the pseudocode for all essential algorithms (Steps 35–41) and (v) the procedure for operating an adaptive light-sheet microscope in a variety of different conditions (including developmental imaging and high-speed functional imaging) and preparing a sample for adaptive imaging (Steps 42–93). As an alternative to augmenting an existing microscope with adaptive imaging capabilities, we provide instructions and a full set of technical drawings for building a replica of our adaptive SiMView light-sheet microscope (Supplementary Data 1). An overview of the protocol and the overall workflow are provided in Fig. 1.

### Principle of operation

As shown in Figs. 1b and 2, the key DOFs of an adaptive SiMView light-sheet microscope with two opposing illumination arms and two opposing detection arms comprise the axial positions of the two detection focal planes ( $D_1$  and  $D_2$ ), the positions of the two light sheets relative to the detection axis ( $I_1$  and  $I_2$ ), the tilt and pivot angles of the two light sheets ( $\alpha_1$  and  $\beta_1$ ,  $\alpha_2$  and  $\beta_2$ ) and the positions of the beam waists of the two light sheets along the illumination axis ( $Y_1$  and  $Y_2$ ). To optimize image quality and maintain the optimal state of the microscope during time-lapse imaging, these ten parameters must be continuously assessed and adapted to the optical properties of the specimen. To do so, diagnostic images are collected in the idle time between consecutive rounds of image volume acquisition to both monitor image quality and quantify possible adjustments required to optimize the microscope state. We acquire image sequences in which  $D_1$ ,  $D_2$ ,  $Y_1$  and  $Y_2$  are varied to correct for detection defocus and to optimally position the light sheets within the sample. Moreover, we use image analysis to compute angles between light sheets and detection focal planes ( $\alpha$  and  $\beta$ ), which allows us to characterize and correct the propagation direction of the light sheets inside the sample. All these measurements are combined into a vector of measurements that, together with a vector describing the current microscope state, is used to compute a new corrected microscope state using the constraint graph formalism and constrained quadratic optimization introduced in the AutoPilot framework (see the supplementary materials of Royer et al. for a detailed overview of the AutoPilot theory<sup>21</sup>). This new state vector is then used in subsequent rounds of image acquisition until the microscope has collected enough measurements to apply another update to the state vector.

We note that adjustments to the DOFs  $D$  and  $I$  affect the relative positions of both detection focal planes and light sheets; thus, in theory, only one of the two DOFs is needed to correct for defocus aberrations. However, in practice, there are two important differences that make it very useful to incorporate both of these DOFs into the adaptive microscope. First, varying  $D$  (moving the detection objective while keeping the light sheet stationary) leads to a change in only the sharpness of the image, whereas varying  $I$  (moving the light sheet while keeping the detection objective stationary) additionally leads to a change in image content, as different parts of the specimen are illuminated when displacing the light sheet along the detection axis. Second, the DOF  $D$  is associated with high-precision piezo positioners, which are excellent devices for establishing a precise reference coordinate system for three-dimensional (3D) volume acquisition. In general, such a reference system with well-defined spatial coordinates is required to ensure spatial continuity throughout the volume during 3D image acquisition, and the additional tilt/pivot errors that typically occur in the illumination system make the DOF  $I$  less suitable for this purpose than  $D$ . Thus, defocus *measurements* are best implemented by varying the position of the detection focal plane along the detection axis ( $D$ ), whereas the subsequent defocus *corrections* are best implemented by maintaining a constant  $D$  setting and correcting the position of the light sheets along the detection axis ( $I$ ) to match the positions of the detection focal planes.

### Applications

The SiMView adaptive light-sheet microscope, the AutoPilot control software and the experimental protocols described here have been used extensively for high-resolution, time-lapse imaging of the development of entire zebrafish, *Drosophila melanogaster* and *Parhyale hawaiensis* embryos with a

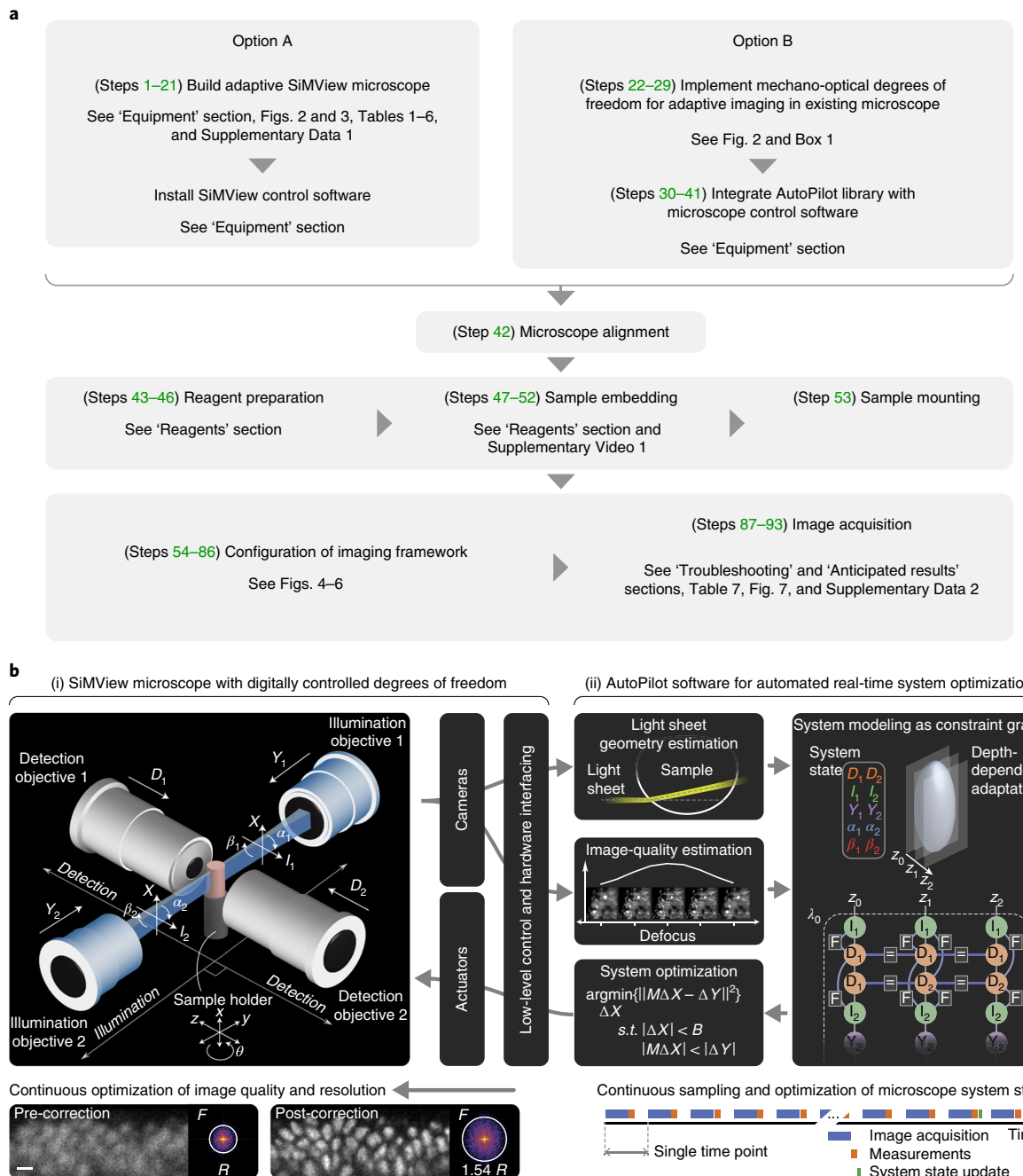


**Fig. 1 | Overview of the protocol and AutoPilot framework.** **a**, Workflow and overview of the main steps of the protocol. To build an adaptive SimView microscope, use option A; to implement mechano-optical DOFs for adaptive imaging in an existing microscope, use option B. **b**, Conceptual overview of the light-sheet microscopy framework for spatiotemporally adaptive imaging. The framework consists of (i) a multiview light-sheet microscope (SiMView) with ten digitally adjustable DOFs that control 3D offsets and 3D angles between light sheets and detection focal planes, and (ii) a real-time software layer (AutoPilot) that autonomously monitors image quality throughout the imaging volume and continuously adjusts these DOFs to optimize spatial resolution and image quality across the sample in space and time. Scale bar, 5  $\mu\text{m}$ . **b** adapted from Royer et al.<sup>21</sup>, Springer Nature Limited.

temporal resolution of 15–60 s<sup>10,21–25</sup>, *in toto* imaging of *Drosophila* nervous system explants<sup>26</sup> and high-speed functional imaging of the zebrafish larval brain, as well as the *Drosophila* embryonic and larval nervous system at volume rates up to 5 Hz<sup>16,21</sup>. In all these imaging applications involving complex multicellular organisms or tissue and organ explants, the AutoPilot framework is a useful tool for improving spatial resolution and signal strength, recovering cellular or even subcellular structures in many regions that cannot be resolved with conventional light-sheet microscopy<sup>21</sup>.

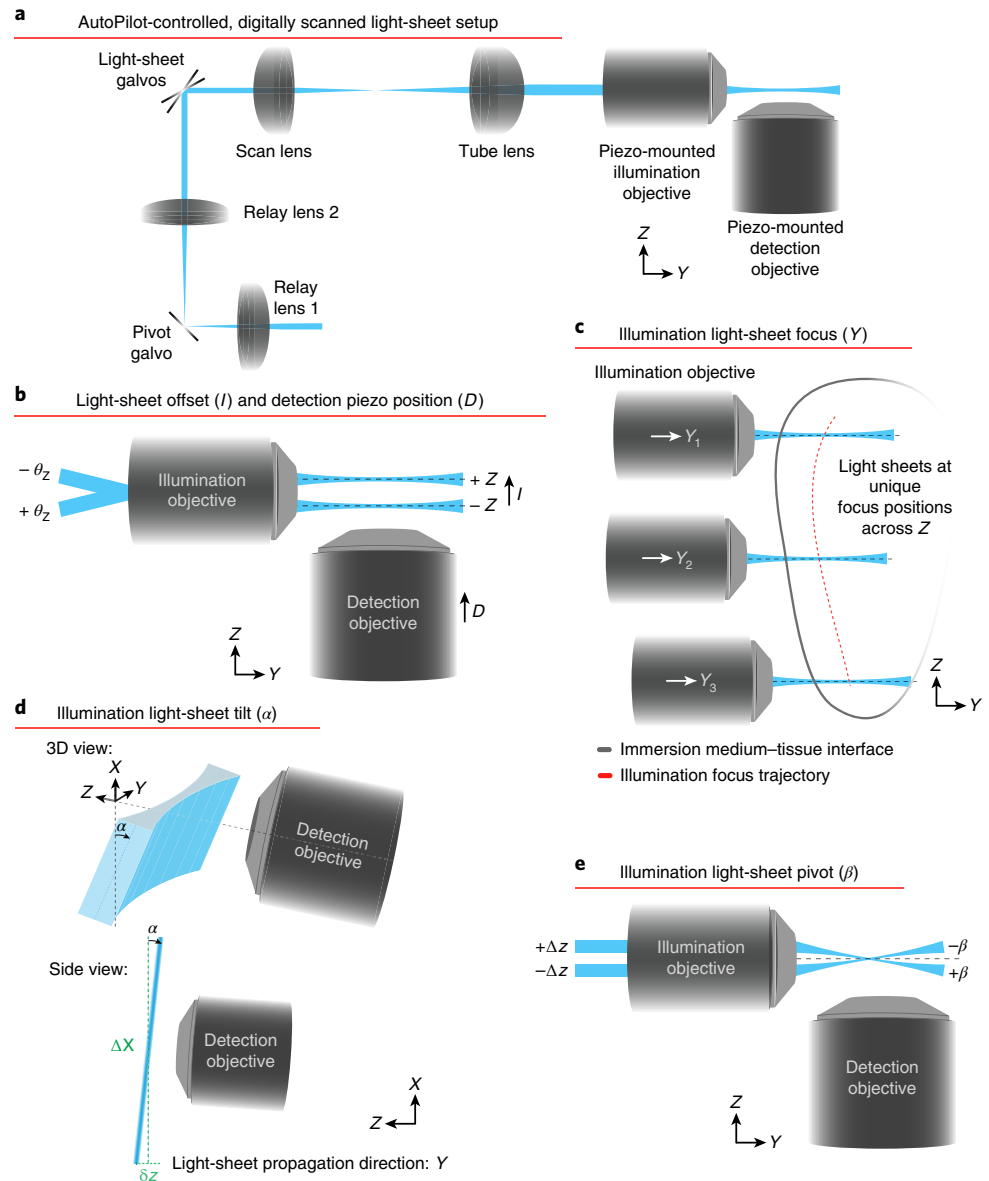


**Fig. 2 | Degrees of freedom of the AutoPilot framework.** **a**, Basic components of a scanned light-sheet microscope for adaptive imaging, consisting of piezo-mounted illumination and detection objectives to control illumination light-sheet focus ( $Y$ ) and detection piezo position ( $D$ ), a dual-axis light-sheet galvo to control light-sheet offset ( $I$ ) and light-sheet tilt ( $\alpha$ ), and a pivot galvo to adjust light-sheet pivot ( $\beta$ ). **b**, Scanning the  $Z$ -mirror in the light-sheet galvo generates the angular tilts ( $\pm\theta_z$ ) at the back focal plane of the objective, which effectively translate to offsets of the scanned light-sheet in the sample plane ( $\pm Z$ ). The detection objective is translated in  $Z$  by a high-speed piezo to overlap the detection focal plane with the light-sheet plane. The light-sheet offset ( $I$ ) and detection piezo position ( $D$ ) are the DOFs adjusted and optimized by the adaptive imaging framework. **c**, The piezo-mounted illumination objective is adjusted in  $Y$  by the adaptive imaging framework during depth sectioning, thereby uniquely positioning the light-sheet foci to adapt to a change in the tissue-medium interface as a function of depth. **d**, The illumination light-sheet tilt ( $\alpha$ ) rolls the light-sheet plane about the axis of beam propagation. This degree of freedom, controlled by the adaptive imaging framework, is generated by the dual-axis light-sheet galvo and allows for an optimal match of the light-sheet plane to the detection plane as a function of  $X$ . **e**, The illumination light-sheet pivot ( $\beta$ ) enables the adjustment of the yaw angle of the light-sheet. This degree of freedom, controlled by the adaptive imaging framework, is generated by the pivot galvo, which offsets the illumination beam in  $Z$  ( $\pm\Delta z$ ) at the back focal plane of the objective, which effectively pivots the beam ( $\pm\beta$ ) in the sample plane.

Applications requiring high spatial resolution thus benefit most from the use of the AutoPilot framework, e.g., when aiming to collect image data for the purpose of cell tracking, measurement of dynamic changes in cell shape, gene expression or protein localization inside the cells of developing

embryos or for whole-brain functional imaging at the single-cell level. We also successfully tested these methods and protocols in other biological model systems, using both structural and functional fluorescent indicators, as well as sparse and dense labeling strategies. In general, the AutoPilot libraries and image analysis algorithms presented here are designed to be robust across a wide variety of imaging conditions and do not make assumptions about the type of specimen, marker strategy or spatiotemporal distribution of fluorescent molecules used for imaging. The SiMView microscope design included in this protocol is suitable for imaging volumes up to  $830\text{ }\mu\text{m} \times 830\text{ }\mu\text{m} \times 3,000\text{ }\mu\text{m}$  without a need for tiling; it also offers a multivolume acquisition feature that can be used to further increase the lateral extent of the imaging volume (via tiling) up to a total size of  $\sim 2,000\text{ }\mu\text{m} \times 3,000\text{ }\mu\text{m} \times 3,000\text{ }\mu\text{m}$ . In the realm of high-speed functional imaging, SiMView offers a temporal resolution of 200 ms for a 200- $\mu\text{m}$ -deep volume (using the PI P-622.1CD stages listed in Table 1), which is large enough to cover, e.g., the brain of a larval zebrafish, an entire *Drosophila* first instar larva or a nervous system explant of a *Drosophila* third instar larva.

### Comparison with other methods

Light-sheet microscopy offers excellent spatial resolution and imaging speed combined with exceptionally low photodamage and light exposure of the specimen<sup>1–4,27</sup>. This unique set of capabilities has been instrumental in enabling a wide range of new live-imaging experiments in the life sciences. For example, the developmental and functional imaging experiments described here and in Royer et al.<sup>21</sup> would not be possible using point-scanning confocal fluorescence microscopy, two-photon microscopy or spinning-disk confocal fluorescence microscopy, because of the lower imaging speed of these techniques and, in the case of confocal microscopy, because of the high energy load on the specimen<sup>28</sup>. Compared with conventional light-sheet microscopes, such as selective plane illumination microscopy (SPIM)- or digital scanned laser light-sheet fluorescence microscopy (DSLM)-type instruments<sup>5,20</sup>, adaptive SiMView light-sheet microscopy offers several advantages. First, the SiMView concept of simultaneously illuminating the specimen and detecting fluorescence along multiple directions enables fast, high-quality imaging of large, partially opaque specimens. Second, the microscope's ability to rapidly adapt itself (via the AutoPilot framework) to the dynamic optical properties of the specimen in both space and time recovers high resolution and maintains optimal image quality during long-term time-lapse image acquisition. An alternative to adaptive imaging with the AutoPilot framework could be to apply such corrections manually before the start of an imaging experiment, or perhaps even during a recording (assuming that the microscope has at least some of the hardware DOFs described in this protocol, such as piezo positioners for translating the detection objectives). This approach is, however, highly impractical and almost always impossible to implement in practice for a number of reasons, including the large number of parameters that must be adjusted, the very short idle time of the microscope between consecutive volume acquisitions, the variability of the required corrections across space and over time and the need for rapid and objective assessment of the quality of complex, mega-pixel images. Moreover, the attempt to apply manual corrections would inevitably expose the specimen to much more light than what is needed for the automated measurements performed by the AutoPilot framework.

However, variations of the optomechanical implementation and the automated adaptive imaging strategy described here are conceivable. For example, spatial light modulators and deformable mirrors integrated into the illumination and/or detection arms of the microscope design described here could be used to correct for higher-order aberrations (see a discussion on this in the 'Limitations' section below). An alternative microscope design that focuses on higher-order aberration correction and addresses a complementary application space has been described in literature<sup>29</sup>. Specifically, this latter design, termed AO-LLSM (adaptive optical lattice light-sheet microscopy), has the potential to offer even higher spatial resolution but limits the field of view to only 30–60  $\mu\text{m}$  along all three dimensions (as compared with 830  $\mu\text{m}$  in the design described here), as a direct result of the small size of isoplanatic patches in typical biological specimens. AO-LLSM applications thus focus on the imaging of individual cells or small subvolumes of multicellular organisms. Moreover, AO-LLSM is more sensitive to scattered light and has thus been primarily used in zebrafish embryos, which exhibit only mild light scattering. In theory, the imaging of larger volumes could be implemented in the context of AO-LLSM (if the specimen is largely transparent), but this approach would require tiling and sequential acquisition of small, individually corrected subvolumes, which greatly reduces imaging speed and compromises typical applications of

**Table 1 | Components of the AutoPilot modules and SiMView light-sheet microscope**

Module	Component	Product(s)	Manufacturer
Optical table and breadboard	Optical table	ST-UT2-48-8 optical table (4 feet × 8 feet × 8 inches), with S-2000 series 28-inch isolators with automatic leveling and S-2000A-428 (4×), IQ-200-UG-8 damper upgrade	Newport
	Breadboard	Custom RG breadboard 04SI69108 (2.0 feet × 5.0 feet × 2.4 inches)	
	Rail system	SYS 40 and SYS 65 rail and slide system components	OWIS
Lasers	SOLE-3 engine with dual-fiber head	Solid-state lasers: 488 nm, 561 nm and 594 nm	Omicron Laserage
Illumination subsystems (two modules)	Mechanical parts	J007264 laser collimator	Custom design
	High-speed laser shutter	VS14S2ZM1-100 with AlMgF2 coating	Uniblitz
	Illumination filter wheel	VMM-D3 three-channel driver 96A351 filter wheel MAC6000 DC servo controller NDQ neutral-density filters Laser cleanup notch filters: 488/10, 561/10 and 594/10	Ludl Melles Griot Chroma
	Relay lens pair	49-361-INK (2×)	Edmund Optics
	<b>Dual-axis laser scanner (2×)</b>	<b>6215HSM40B galvanometer scanner</b> <b>MicroMax 673XX dual-axis integrating servo driver amplifier</b> <b>6-mm XY mirror set, mount and interconnect cables</b> <b>MK320S-24 power supply</b>	<b>Cambridge Technology</b>
Detection subsystems (two modules)	F-theta lens	66-S80-30T-488-1100nm	Astrodyne
	Tube lens	49-360-INK	Custom design (built by Special Optics)
	<b>Piezo positioner for illumination objective</b>	<b>P-628.1CD PI Hera piezo linear stage</b> <b>E-665 piezo amplifier and servo controller</b>	Edmund Optics
	Illumination objective	Plan Fluor 10×/0.30 W	Physik Instrumente
	Mechanical parts	J002551 three-axis piezo mount J002560 string plunger J007259 illumination objective assembly J007265 objective flexure J001536, J001537 galvo assemblies J007260 mirror mounts J005858, J005859 and J007263 adjustable optic mounts J007267, J007268 illumination shutter and filter assemblies	Nikon
Detection subsystems (two modules)	Detection filter wheel	96A354 filter wheel MAC6000 DC servo controller	Custom design
	Detection filter wheel	RazorEdge and EdgeBasic long-pass filters: 488 nm, 561 nm and 594 nm BrightLine band-pass filters: 525/50 nm	Ludl
	Tube lens module	CFI second lens unit AxioImager 130-mm ISD tube lens	Semrock
	<b>Piezo positioner for detection objective</b>	<b>P-622.1CD PI Hera piezo linear stage</b> <b>E-665 piezo amplifier and servo controller</b>	Nikon
	Detection objective	CFI60/75 LWD water-dipping series Apochromat/Plan-Apochromat water-dipping series	Carl Zeiss
Camera	Camera	Orca Flash 4.0 v2 camera JULABO water chiller	Physik Instrumente
	Mechanical parts	J002422 three-axis piezo mount J002560 spring plunger J005856 filter wheel assembly J007258 detection objective assembly	Nikon
			Carl Zeiss
			Hamamatsu
			Custom design

Table continued

**Table 1 (continued)**

Module	Component	Product(s)	Manufacturer
Specimen chamber	<i>Four-view specimen chamber</i>	J007262 camera assembly J007266 detection flexure	Custom design
	<i>Specimen holder</i>	J007055 chamber assembly (black Delrin) J002170 seal ring <i>J002171 collet holder</i> <i>J002289, J002290 and J002291 plastic collets to hold glass capillaries with a sample embedded in agarose</i>	
Specimen positioning system	Translation stages (3×)	M-111K046	Physik Instrumente
	Rotary stage	M-116.2DG	
Real-time electronics	Motion I/O interface and amplifier	C-809.40 four-channel servo-amplifier	National Instruments
	Motion controller	PXI-7354 four-axis stepper/servo motion controller	
Control software	<i>Mechanical parts</i>	J005962 sample-stage assembly	Custom design
	PXI chassis	PXI-1042	
Microscope control workstation	Real-time controller with LabVIEW Real-Time OS	PXI-8110 Core 2 Quad, 2.2 GHz	National Instruments
	I/O interface boards (4×)	PXI-6733 high-speed analog output eight-channel board	
Control software	BNC connector boxes (4×)	BNC-2110 shielded connector block	Custom software
	Serial interface board	PXI-8432/2	
Microscope control workstation	Real-time modules	32-bit LabVIEW code	Custom software and third-party libraries
	Host modules	64-bit LabVIEW code	
Microscope control workstation	AutoPilot modules	Java 8 code C interface library code Third-party libraries <sup>1</sup>	Colfax International
	SX6750 microscope control and data acquisition workstation <sup>2</sup>	Intel Xeon E5-2687W CPUs (2×) 16-GB DDR-3 RAM modules (16×) 16-channel Intel RS2WG160 RAID controller Intel 520 Series 480-GB SSDs (2×) Western Digital 2.5 XE 900-GB HDDs (14×) Firebird CameraLink frame grabbers (2×) Intel AXRSBBU8 battery backup Intel X520-SR1 SFP + SR LC fiber network adapter PNY nVidia Quadro 2000D graphics card	

This table contains a comprehensive list of optical parts, mechanical parts, electronics and computational hardware used to build a custom SiMView-type light-sheet microscope for spatiotemporally adaptive imaging. Custom mechanical designs associated with each microscope module are shown in italic and the modules used by the AutoPilot framework are shown in bold.

<sup>1</sup>Third-party libraries used in the AutoPilot framework include the following code modules: com.googlecode.efficient-java-matrix-library:ejml:0.24, com.github.rwl:jtransforms:2.4.0, org.apache.commons:commons-collections4:4.4+, commons-io:commons-io:2.4+, org.apache.commons:commons-lang3:3.1, net.sf.trove4j:trove4j:3.0.3, org.apache.commons:commons-math3:3.2, org.jzy3d:jzy3d-api:0.9.1, commons-beanutils:commons-beanutils:1.7.0, 'javassist:javassist:3.0, commons-digester:commons-digester:1.8, 'jdepend:jdepend:2.9.1, commons-logging:commons-logging:1.1.1, 'java3d:vecmath:1.3.1, net.sourceforge.csparse:csparsej:csparsej:1.1.1, args4j:args4j:2.0.29, org.codehaus.groovy:groovy-all:2.2.2

<sup>2</sup>Minimum hardware requirements of the control and data acquisition workstation when using the SiMView control framework and SiMView microscope hardware: Intel CPU with at least four cores per camera and 3-GHz clock speed (required by the Orca Flash cameras), 32-GB memory per camera, storage system supporting 800 MB/s sustained write speed per camera and sufficient capacity for the desired duration of imaging experiments. Minimum hardware requirements for the AutoPilot libraries: To provide adequate data throughput in a SiMView-type microscope, the AutoPilot library requires a computer system with at least 16 CPU cores (possibly shared across two CPUs) and a base frequency of at least 3 GHz. As the AutoPilot core library makes extensive use of multithreading to accelerate computation, increasing the number of total cores is the most effective approach to increasing performance.

large-volume light-sheet microscopy, such as cell tracking or high-speed functional imaging across large cell populations.

### Expertise needed to implement the protocols

The protocols detailed here require some prior experience in building (or modifying) light microscopes and programming or software development. The most effective and time-efficient implementation of these protocols is achieved through involvement of (i) a physicist or optical engineer who is familiar with building optical instruments, ideally light-sheet microscopes, and has some prior experience in using electronics for hardware control and automation; (ii) a computer scientist or software engineer with experience in Java, C++ and/or LabVIEW; and (iii) a biologist or experienced

microscopist with practical knowledge of sample preparation for fluorescence microscopy and the operation of light microscopes.

### Limitations

The highest potential for improving image quality and spatial resolution using adaptive imaging techniques is realized in samples that are relatively transparent. Image quality in highly light-scattering samples will generally be poor in any light-sheet microscope, with or without adaptive imaging capabilities, as none of the mechanisms and DOFs discussed here (Fig. 2) are designed to address the stochastic light diffusion introduced by light scattering. We note that the use of line-confocal detection<sup>30–33</sup> is a complementary strategy that can partially counteract the degradation in image quality arising from light scattering and synergizes with the methods described here.

Moreover, our framework is designed to correct for first-order and some second-order aberrations (tip/tilt, defocus) in the illumination and detection paths of a light-sheet microscope. It does not address higher-order aberrations. In practice, tip/tilt and defocus are the most harmful aberrations in light-sheet microscopy if left unaccounted for, and their elimination is typically a prerequisite for effectively dealing with higher-order aberrations. We found that higher-order aberration correction is usually not required to recover cellular resolution (e.g., the ability to recognize neighboring cells as distinct objects when using nuclear fluorescent labels) in those specimen regions where aberration correction alone is a viable strategy for improving image quality, considering that light scattering would otherwise dominate image-quality degradation anyway (e.g., at depths beyond ~60 µm in fruit fly embryos or ~100 µm in zebrafish embryos). However, if subcellular resolution down to a few hundred nanometers is desired, the introduction of additional mechanisms for higher-order aberration correction, e.g., use of spatial light modulators and deformable mirrors, may become necessary.

Finally, the protocols provided below consider two primary scenarios: the upgrade of an existing light-sheet microscope or the implementation of an adaptive SiMView light-sheet microscope. In this context, we note that SiMView microscopy belongs to the family of scanned light-sheet microscopy (DSLM)<sup>5</sup>, which generates a light sheet through one-dimensional laser scanning of a Gaussian beam illuminating the specimen from the side. Compared with the alternative approach of using a light sheet generated with a cylindrical lens (SPIM), there are several implications for imaging performance. The advantages of DSLM over SPIM are that DSLM reduces shadowing artifacts<sup>34</sup> (through the intrinsically incoherent illumination scheme; by contrast, SPIM requires an additional pivoting mechanism to address this issue<sup>35</sup>) and enables confocal line detection<sup>30–33</sup> as well as the use of efficient two-photon excitation<sup>36</sup>, Bessel plane illumination<sup>37</sup> and efficient structured illumination<sup>6</sup>. The latter feature greatly benefits adaptive imaging (and is integrated into the SiMView control framework discussed here as an optional mode of operation), as it introduces an engineered high-frequency component into the image data that maximizes the robustness of autofocusing independently of the native image content<sup>21</sup>. The associated intensity-modulated illumination pattern also reduces energy load on the specimen during autofocusing by a factor of 2. The advantage of SPIM over DSLM is that it reduces peak illumination power (while using the same integrated illumination light energy for images of equal brightness). If the latter feature is required, we note that this does not prohibit the use of the adaptive imaging framework described here. All adaptive imaging DOFs are compatible with a SPIM-based microscope design and can be implemented in such a system in the same way as described here for a DSLM-type microscope.

### Experimental design

In this section, we will discuss some experimental aspects that should be considered before following the instructions in this protocol.

### Implementation of microscope hardware

The most time-consuming step involved in building a copy of the adaptive SiMView light-sheet microscope or integrating the AutoPilot hardware modules into an existing microscope is the wait time until the arrival of new hardware components. While most of the smaller required items are relatively easily and quickly obtained, the lead time for some of the more complex and expensive components listed in Table 1 can be up to 3–4 months. When building the full microscope described in Steps 1–21 of the protocol, the items with the longest lead time will typically be the optical table, laser system, custom f-theta lens, motorized stages, piezo positioners, galvanometer scanners and cameras. Moreover, the lead time for fabrication of custom mechanical components described in

Supplementary Data 1 can vary from a few weeks to several months, depending on the vendor and its workshop's current workload. When integrating AutoPilot hardware modules into an existing microscope (Table 1; commercial components are shown in bold; custom mechanical components are shown in italic), the items with the longest lead time will be the piezo positioners, galvanometer scanners and potentially some of the custom mechanical parts.

### Compatibility of the AutoPilot framework with existing microscope designs

The AutoPilot framework described here is compatible with any light-sheet microscope design that uses independent optical components for light-sheet illumination and fluorescence detection (assuming that the capability to digitally adjust the position of these components is either already available or can be added to the system, e.g., through the use of piezo positioners) or, alternatively, that provides remote focusing functionality such that light sheet(s) can be moved independently of detection focal plane(s). This means that the AutoPilot framework can be integrated, e.g., in SPIM<sup>20</sup>, DSLM<sup>5</sup>, SiMView<sup>7,16</sup>, MuVi-SPIM<sup>8</sup>, IsoView<sup>17</sup>, Bessel plane illumination<sup>37,38</sup> or lattice light-sheet microscopes<sup>39</sup>. Single-objective microscope designs, such as those used in oblique plane microscopy<sup>40</sup> and SCAPE<sup>41</sup>, would require additional hardware upgrades (such as components for selective adjustability of light-sheet position and orientation or remote focusing functionality in the detection arm) to be able to support AutoPilot functionality.

The AutoPilot framework, including the DCTS (Shannon entropy of the normalized discrete cosine transform) focus metric and the focusing algorithms, makes no assumptions about the type of light-sheet illumination used in the microscope and is thus compatible with Gaussian sheets<sup>20</sup>, scanned Gaussian beams<sup>5</sup>, scanned Bessel beams<sup>37,38</sup> and dithered optical lattices<sup>39</sup>, just to name few commonly used methods. Similarly, owing to the robustness of the AutoPilot image-processing routines to noise, the method can be integrated in both one-photon and multiphoton<sup>7,36,42</sup> imaging assays.

## Materials

### Biological materials

- *Drosophila* transgenic strain w; His2Av-mRFP1; + (Bloomington Stock Center, stock no. 23651)
- Zebrafish transgenic strain *Tg(β-actin2:H2B-eGFP)* (Janelia Research Campus, stock no. 2131 (contact P.J.K., kellerp@janelia.hhmi.org))

### Reagents

- Low-melting-temperature agarose (Seaplaque; Lonza, cat. no. 50100)
- Physiological saline for isolated *Drosophila* nerve cords<sup>16</sup> (Reagent setup)
- Soft wax (Utility Wax; Darby Dental Supply, cat. no. 0928094)
- NaCl (Sigma Aldrich, cat. no. 746398)
- KCl (Sigma Aldrich, cat. no. P5405)
- CaCl<sub>2</sub>·2H<sub>2</sub>O (Sigma Aldrich, cat. no. C5080)
- MgCl<sub>2</sub>·6H<sub>2</sub>O (Sigma Aldrich, cat. no. M2693)
- TES (Sigma Aldrich, cat. no. T6541)
- Sucrose (Sigma Aldrich, cat. no. S7903)
- NaOH (Sigma Aldrich, cat. no. S8045)

### Equipment

#### Equipment for sample preparation

- Glass capillary tubes, length 2.0 cm, o.d./i.d. 2.0/1.5 mm or 3.0/2.5 mm (Hilgenberg, custom order)
- Agarose-coated 100-mm culture dish (Fisher Scientific, cat. no. 08-772E)
- Pipette tips cut to snugly hold the capillary tubes (Eppendorf, cat. no. 022491938)
- Pipettor (200 μm; Eppendorf, cat. no. 3123000055)
- Fine forceps (Dumont no. 5; Fine Science Tools, cat. no. 1125240)
- Small (35-mm) culture dish for holding embedded samples in aqueous medium (Fisher Scientific, cat. no. 12-600-000)

#### Equipment for AutoPilot modules and SiMView light-sheet microscope

- Hardware components of AutoPilot modules and SiMView light-sheet microscope (Table 1)
- ▲ **Critical** A comprehensive list of optical parts, mechanical parts, electronics and computational

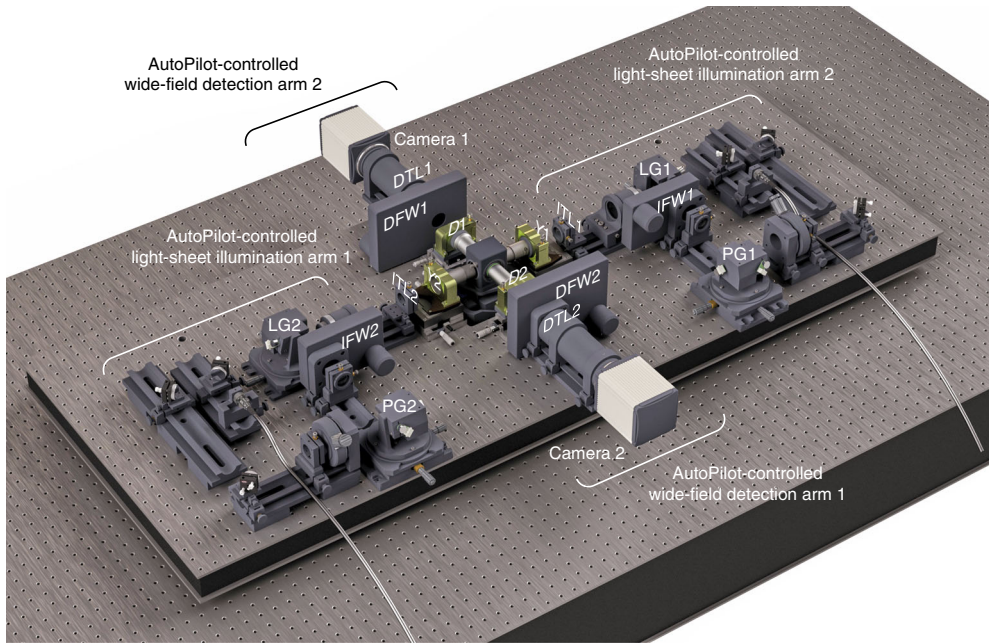


**Fig. 3 | Implementation example of adaptive multiview light-sheet microscopy.** Computer model of the adaptive SiMView light-sheet microscope. Detailed technical drawings for all components used in this microscope implementation are provided in Supplementary Data 1. DTL, detection tube lens; DWF, detection filter wheel; IFW, illumination filter wheel; ITL, illumination tube lens; LG, light-sheet galvanometer scanner; PG, pivot galvanometer scanner. Y (piezo positioners for illumination objectives) and D (piezo positioners for detection objectives) refer to the respective DOFs of the AutoPilot framework.

hardware used to build a custom SiMView-type light-sheet microscope for spatiotemporally adaptive imaging (Fig. 3) is provided in Table 1. Custom mechanical designs associated with each microscope module are shown in italic and the modules used by the AutoPilot framework are shown in bold. Note that the AutoPilot modules serve as independent modules that can also be incorporated into other types of light-sheet microscopes. In this latter scenario, only the parts shown in bold are relevant for retrofitting an existing microscope. The total cost for all parts listed in Table 1 is approximately US \$280,000 (corresponding to a complete adaptive SiMView microscope), whereas the cost for parts needed for an AutoPilot upgrade for an existing microscope ranges between US \$25,000 and US \$50,000, depending on the number of illumination and detection arms in the microscope (considering two arms in total at the lower end of the range and four arms in total at the upper end). This latter cost estimate assumes that one high-performance piezo positioner is added to each illumination or detection arm to enable precise, digitally controlled positioning of the respective objective (DOFs *D* and *Y*), and that two dual-axis galvanometer scanners are added to each illumination arm (DOFs *I*,  $\alpha$  and  $\beta$ ). If some of these components are already present in the microscope, costs are reduced accordingly. The most expensive items on the parts list for the SiMView microscope are the optic table, multiwavelength laser system, high-performance piezo positioners, cameras, motorized stages, objectives and custom f-theta lenses, as well as computer hardware and electronics. We note that a substantial reduction in cost is feasible for almost all components by choosing lower-cost alternatives that sacrifice some performance. ▲ **CRITICAL** The custom mechanical designs include some parts with high complexity, in particular the three-axis piezo mounts and objective flexures. Custom designs for these parts were necessary in order to create a low-profile stage assembly that is more compact and versatile than commercially available products. Specifically, our design ensures that (i) the overall weight atop the piezo stage can be kept to a minimum while still maintaining the necessary translation and angular adjustments (*Y*, *Z* and yaw adjustment are achieved using the stage that sits underneath the piezo itself); (ii) four objective mounts can be positioned around the chamber without obstruction; (iii) the objective can be translated in *X*, *Y* and *Z*; (iv) the yaw angle of the objective can be adjusted by differentially adjusting the micrometers on the stage; (v) reproducibility can be maintained when the objectives must be removed from the chamber; (vi) alignment can be maintained when objectives must be swapped out, as different objectives can attach to the same flexure via different adapters; and (vii) all DOFs are implemented in a system that is sufficiently compact to be compatible with the

OWIS SYS65 rail system used in the SiMView microscope. Similarly, custom parts are used when off-the-shelf components cannot provide the necessary integration into the optical rail system used in the microscope.

### Software

- AutoPilot software (<https://microscopeautopilot.github.io/>)
- GIT (<https://git-scm.com/>)
- Java 8 (<https://java.com/en/download/>)
- LabVIEW (optional, relevant only to building the SiMView-type adaptive light-sheet microscope; <http://www.ni.com/en-us/shop/labview.html>) ▲ **CRITICAL** The following modules are required: LabVIEW 2015 SP1 (or higher) 64-bit (for the host computer), LabVIEW 2015 SP1 (or higher) 32-bit (for communication with the real-time target), LabVIEW Real-Time Module 2015 SP1 (or higher), LabVIEW Vision Development Module 2015 SP1 (or higher), LabVIEW Vision Acquisition Software August 2015 f1 (or higher), LabVIEW SoftMotion Module 2015 SP1 f1 (or higher), NI 845 × 15.0 (or higher), NI Motion 15.0 (or higher) and NI Device Drivers 2015 (or higher).
- SiMView light-sheet microscope control software (optional; only relevant to building the SiMView-type adaptive light-sheet microscope): a free license for the LabVIEW-based microscope control framework can be obtained via a Material Transfer Agreement through the Janelia Open Science portal (<https://www.janelia.org/open-science>) or by contacting P.J.K. (kellerp@janelia.hhmi.org).

### Reagent setup

#### Agarose

To prepare a 1% (wt/vol) solution of agarose, add 1.0 g of agarose powder to 100 mL of water in a Pyrex bottle or flask. Mix well and heat with a hot plate or microwave oven until the solution boils. The solution will be clear at this point with no visible undissolved agarose. Aliquots of agarose solution can be kept at 4 °C for 3 months. Heat the solid agarose to 80 °C in a heating block to liquefy and use within 12 h.

#### Physiological saline

For isolated *Drosophila* nervous systems, the agarose should be dissolved in physiological saline as shown in the table below.

NaCl	135 mM
KCl	5 mM
CaCl <sub>2</sub> ·2H <sub>2</sub> O	2 mM
MgCl <sub>2</sub> ·6H <sub>2</sub> O	4 mM
TES	5 mM
Sucrose	36 mM
Adjust the pH to 7.15 with 10 N NaOH	

▲ **CRITICAL** This saline keeps the larval CNS healthy and active for as long as 2 h<sup>16</sup>. Store the saline at 4 °C for up to 2 weeks. Aliquots of agarose in physiological saline can be stored at 4 °C for up to 2 weeks. Heat the solid agarose to 80 °C to liquefy and use within 1 h.

### Equipment setup

#### GIT

To install GIT on your computer, follow the instructions here: <https://git-scm.com/>.

#### AutoPilot software

Use GIT to clone the repository as explained here: <https://github.com/MicroscopeAutoPilot/AutoPilot/wiki/howtobuild>.

#### Java

To install Java 8 (JDK 8), follow the instructions here: <https://java.com/en/download/>.

#### (Optional) LabVIEW

To purchase and install LabVIEW on your computer, follow the instructions here: <http://www.ni.com/en-us/shop/labview.html>.

**Procedure****Implementation of the light-sheet microscope** ● **Timing** 1–2 weeks

▲ **CRITICAL** The first section of this protocol describes the implementation of the light-sheet microscope (Steps 1–21), in which the adaptive imaging capabilities will be introduced. Specifically, we describe the construction of a SiMView light-sheet microscope<sup>7,21</sup> as a basis for the adaptive imaging framework (Fig. 3). If using an existing microscope design, proceed directly to Step 22.

▲ **CRITICAL** All assembly and part drawings referenced in the instructions below are provided in Supplementary Data 1. The respective CAD models for the parts are also provided. Information on the analog and digital channel configuration of the PXI devices is provided in Tables 2–6.

- 1 Mount the custom breadboard (Newport, 04SI69108) with a cutout hole (part drawing PG-25-2-ML) onto the optical table (Newport, ST-UT2-48-8), as shown in assembly drawing J007042.
- 2 Attach the illumination and detection OWIS rails (part drawings J006370 and J007043, respectively) to the custom breadboard, leaving ~3.5–3.75 inches from the edge of the cutout hole, as shown in assembly drawing J007042. Use a straight-edge ruler and an L-square as guides to mount the rails for parallel and orthogonal alignments, respectively.
- 3 Assemble the specimen-positioning system, comprising three single-axis linear translation stages (Physik Instrumente, M-111K046) and a rotary stage (Physik Instrumente, M-116.2DG), as shown in assembly drawing J005962. Insert this specimen-positioning assembly through the rectangular cutout hole on the breadboard and attach it to the optical table.
- 4 Attach the sample mount (part drawing J002171), using the precision magnetic beads on its underside, to the sample shaft (part drawing J005968) of the specimen-positioning assembly.
- 5 Affix the specimen chamber (assembly drawing J007055) to the chamber support (part drawing J005963) of the specimen-positioning assembly (assembly drawing J005962), such that the larger holes for the detection objectives are along the short axis of the optical table. Insert the sample mount (part drawing J002171) through the sample seal (part drawing J002169).
- 6 Assemble a pair of detection objective units and illumination objective units as shown in assembly drawings J007258 and J007259, respectively. Insert the objectives through their respective flexible imaging seals (part drawings J002966 and J002967) in the specimen chamber.
- 7 Assemble the detection tube lens and camera as shown in assembly drawing J007262.
- 8 Attach the detection filter wheel (Ludl, 96A354) to a mount (part drawing J002543) as shown in assembly drawing J005856. Mount the detection filter wheels on the detection OWIS rails (part drawing J007043) followed by the detection tube lens-camera assembly, as shown in assembly drawing J007042.
- 9 Mount the illumination tube lens (Edmund Optics, 49-360-INK; mount: assembly drawing J007263) and scan lens (Special Optics, 66-S80-30T-488-1100; mount: part drawing J005982) on the illumination rails (part drawing J006370) as shown in assembly drawing J007042.
- 10 Assemble the four dual-axis galvo scanners (Cambridge Technology, 6215HSM40B), as shown in assembly drawings J001536 and J001537. Select two opposite-handed galvos as light-sheet scanners and position them before the scan lenses as shown in assembly drawing J007042.
- 11 Use the other two dual-axis galvo scanners (Cambridge Technology, 6215HSM40B) as pivot scanners and position them between a pair of relay lenses (Edmund Optics, 49-361-INK), such that the focal planes of these lenses overlap with the Y-mirror in the dual-axis galvo scanner. The entrance and exit beams at the galvo have different heights, so mount the lenses before and after the pivot scanners as shown in assembly drawings J005858 and J005859, respectively.
- 12 Attach the high-speed laser shutter (Uniblitz, VS1422ZM1-100) to a mount (part drawing J002528), as shown in assembly drawing J007267. Position it before the pivot scanner, as shown in assembly drawing J007042.
- 13 Attach the illumination filter wheel (Ludl, 96A351) to a mount (part drawing J007050), as shown in assembly drawing J007268. Mount the illumination filter wheel on a rail before the light-sheet galvos.
- 14 Attach the fiber from the laser unit (Omicron Laserage, SOLE-3) to the laser collimator, as shown in assembly drawing J007264. Use turn mirrors, as shown in assembly drawing J007260, to align the laser beam as it enters the pivot scanner in the illumination path.
- 15 Configure a chassis (National Instruments, PXI-1042) with (i) a real-time controller (National Instruments, PXI-8110) for real-time and deterministic input/output control of the microscope's electronic components; (ii) three analog output boards (National Instruments, PXI-6733), each connected to a BNC connector box (National Instruments, BNC-2110), to supply analog voltages to

**Table 2 | Channel configuration of PXI I/O device no. 1 in the SiMView light-sheet microscope**

PXI-6733 no. 1	Channel no.	Description	Input or output
Analog channels	0	Light-sheet galvo no. 1 X	Out
	1	Light-sheet galvo no. 1 Z	
	2	Laser power [ $\lambda_1$ ]	
	3	Laser power [ $\lambda_2$ ]	
	4	Laser power [ $\lambda_3$ ]	
	5	Illumination objective no. 1 piezo	
	6	Detection objective no. 1 piezo	
	7	Camera no. 1 trigger	
Digital channels	0	Laser enable [ $\lambda_1$ ]	Out
	1	Laser enable [ $\lambda_2$ ]	
	2	Laser enable [ $\lambda_3$ ]	
	3	Laser shutter no. 1	
	6	Camera no. 1 ready	In

**Table 3 | Channel configuration of PXI I/O device no. 2 in the SiMView light-sheet microscope**

PXI-6733 no. 2	Channel no.	Description	Input or output
Analog channels	0	Light-sheet galvo no. 2 X	Out
	1	Light-sheet galvo no. 2 Z	
	2	Laser power [ $\lambda_4$ ] <sup>*</sup>	
	3	Laser power [ $\lambda_5$ ] <sup>*</sup>	
	4	Laser power [ $\lambda_6$ ] <sup>*</sup>	
	5	Illumination objective no. 2 piezo	
	6	Detection objective no. 2 piezo	
	7	Camera no. 2 trigger	
Digital channels	0	Laser enable [ $\lambda_4$ ] <sup>*</sup>	Out
	1	Laser enable [ $\lambda_5$ ] <sup>*</sup>	
	2	Laser enable [ $\lambda_6$ ] <sup>*</sup>	
	3	Laser shutter no. 2	
	6	Camera no. 2 ready	In

<sup>\*</sup>Channels for additional lasers.

**Table 4 | Channel configuration of PXI I/O device no. 3 in the SiMView light-sheet microscope**

PXI-6733 no. 3	Channel no.	Description	Input or output
Analog channels	0	Pivot galvo no. 1 X	Out
	1	Pivot galvo no. 1 Z	
	2	Pivot galvo no. 2 X	
	3	Pivot galvo no. 2 Z	

modulate the laser power, scan the galvos, translate the piezos and externally trigger the cameras for acquisition of frames; the digital output lines of the BNC-2110 box are used to turn the lasers on/off and to open/close the laser shutters, and the digital input lines are used to monitor the camera-ready-for-trigger pulses output by the cameras; (iii) a PXI serial interface board (National Instruments, PXI-8432/2) to control illumination and detection filter wheels via the servo

**Table 5 | Channel configuration of the PXI serial interface in the SiMView light-sheet microscope**

PXI-8432/2 serial interface	Port no.	Controller axis	Description
	1	1	Illumination filter wheel no. 1
		2	Detection filter wheel no. 1
	2	1	Illumination filter wheel no. 2
		2	Detection filter wheel no. 2

**Table 6 | Channel configuration of the PXI motion controller in the SiMView light-sheet microscope**

PXI-7350 motion controller	Axis	Description
	1	Sample translation X
	2	Sample translation Y
	3	Sample translation Z
	4	Sample rotation

controllers (Ludl, MAC6000) and (iv) a PXI motion controller card (National Instruments, PXI-7350) to control the translation and rotary stages in the specimen-positioning unit.

- 16 Connect the translation and rotary stages to the four-channel input/output (I/O) interface for the motion controller (Physik Instrumente, C-809.40). Connect the I/O interface to the motion controller card (National Instruments, PXI-7350) on the chassis.
- 17 Connect each pair of filter wheels to a servo controller (Ludl, MAC6000). Connect the servo controllers to the serial interface board (National Instruments, PXI-8432/2) on the chassis.
- 18 Connect the piezo linear stages (Physik Instrumente, P-622.1CD and P-628.1CD, for illumination and detection, respectively) to the piezo controllers (Physik Instrumente, E-665). Connect the piezo controllers to the PXI-6733 analog output module via the BNC-2110 connector box.
- 19 Connect the shutters to a shutter controller (Uniblitz, VMM-D3). Connect the shutter controller to the PXI-6733 analog output module via the BNC-2110 connector box.
- 20 Follow the pin diagram from the galvo manufacturer to wire the galvos to the power supply. Heat-sink the galvo drivers (Cambridge Technology, Micromax 673 dual-axis drivers) to allow the dissipation of excess heat to keep the galvos within their operating temperature range. Connect the drivers to PXI-6733 analog output modules via the BNC-2110 connector box.
- 21 Insert frame grabbers (Active Silicon, 1xCLD-2PE8) for the Hamamatsu cameras (Orca Flash 4.0 v2) into the PCIe slots on the control PC. Use camera link cables to connect the frame grabbers to the cameras. Disable CPU C-states, Intel SpeedStep and NUMA optimization in the basic I/O system (BIOS) of your control PC (if applicable).

#### Hardware implementation of the adaptive light-sheet microscope modules ● Timing 8 d

**▲ CRITICAL** This section describes five hardware modules that introduce different DOFs in the adaptive light-sheet microscope (Fig. 2). Each module is optional, but some require common mechanical or electronic adjustments to the microscope. Perform the following steps as needed for your experimental setup: Steps 22 and 23 to implement the detection focus module (hardware module *D*), Steps 24 and 25 to implement the light-sheet *Y* module (hardware module *Y*), Steps 26 and 27 to implement the light-sheet focus module (hardware module *I*), Step 28 to implement the light-sheet  $\alpha$  module (hardware module  $\alpha$ ), and Step 29 to implement the light-sheet  $\beta$  module (hardware module  $\beta$ ).

- 22 *Hardware module D* (Steps 22 and 23). Mount the detection objectives on digitally controlled piezo positioners. The detection piezos establish control of the *D* DOFs (Fig. 2b). Using an additional manual stage for adjustments of the mechanical range is recommended.

**▲ CRITICAL STEP** The piezo that translates the detection objective should have a travel range that covers at least the expected defocus range induced by the sample and mounting media. In the case that 3D imaging is to be performed by piezo scanning instead of stage scanning, the detection piezo

should cover at least the entire axial extent of the sample. Moreover, the sample chamber sealing must be adapted to accommodate the movement of the objectives. For example, O-rings, 3D printed gaskets or molded silicone gaskets can be used to maintain water immersion of the sample and objectives.

- 23 Connect the piezo controller analog inputs (typically in the range of 0–10 V) to distinct analog outputs on a National Instruments data acquisition (DAQ) board for interfacing with the control computer.

- 24 *Hardware module Y* (Steps 24 and 25). Mount the illumination objectives on digitally controlled piezo positioners. The illumination piezos establish control of the Y DOFs (Fig. 2c). Using an additional manual stage for adjustments of the mechanical range is recommended.

▲ **CRITICAL STEP** The piezo for translating the illumination objective should have a travel range that covers at least half of the maximum illumination path length inside the sample. As with the detection piezos, the sample chamber sealing and gasket must be adapted to accommodate the translation of the objective.

- 25 Connect the analog inputs of the piezo controller (typically in the range of 0–10 V) to different analog outputs on a DAQ board for interfacing with the control computer.

- 26 *Hardware module I* (Steps 26 and 27). Use a pair of galvo mirrors (X-galvo and Z-galvo) to generate a digitally scanned light sheet. The X-galvo executes a sweep of the Gaussian beam to generate a scanned light sheet in the sample plane, and the Z-galvo establishes the DOF for the adjustment of *I* (Fig. 2b).

▲ **CRITICAL STEP** We assume that light sheets are created by laser scanning (such as in DSLM<sup>5</sup> or SiMView<sup>7</sup> microscopy). If, instead, a static light sheet is created, using, e.g., a cylindrical lens, the X-galvo described in this step is not required.

▲ **CRITICAL STEP** If using a dual-axis galvo scanner, ensure that the spacing between the two galvo mirrors is minimized and that the back-focal plane of the objective is made conjugate either to a position midway between the two mirrors or to the mirror that uses a larger tilt angle (typically the galvo for light-sheet sweep has a larger tilt angle, as the sample is oriented with its long axis along this dimension). For a complete conjugation of the two galvo mirrors and the objective back-focal plane, a pair of relay lenses can be used between the two galvo mirrors.

- 27 Connect the galvo controller analog inputs (typically in the range of 0–10 V) to distinct analog outputs on a DAQ board for interfacing with the control computer.

▲ **CRITICAL STEP** For small angles, the ratio of the focal length of the scan lens to the objective/tube lens magnification ( $f_\theta/M$ ) provides the theoretical ‘micron/radian’ factor, and thus relates the lateral extent scanned by the light-sheet galvos in the sample plane ( $\Delta X$  and  $\Delta Z$ ) to the optical angles of the light-sheet galvos ( $\theta_{\Delta X}$  and  $\theta_{\Delta Z}$ ) (Box 1, equation 4). Assuming that the voltage to angle calibration of the galvo mirrors is linear over a typically small angular range used in the microscope, the ‘micron/voltage’ parameter for each galvo can be empirically defined by introducing a scaling factor in ‘radian/volt’ that is then applied to  $f_\theta/M$ . This factor can be determined by redirecting a digitally scanned light sheet to the camera in the detection path, for which both the magnification and pixel size are known, and adjusting the empirical factor to match the measured range covered by the light sheet on the camera.

- 28 *Hardware module α* (Step 28). In a DSLM configuration, controlling the light sheet’s angle  $\alpha$  (Fig. 2d) does not require additional hardware. The X-galvo and Z-galvo are sufficient: when  $\alpha = 0$  only the X-galvo is scanning, whereas for  $\alpha \neq 0$ , the Z-galvo is scanning simultaneously to introduce a tilt.

- 29 *Hardware module β* (Step 29). To establish the DOF for adjusting  $\beta$  (Fig. 2e), the yaw angle of the light sheet in the sample plane, add a galvo mirror at the focal plane of a pair of relay lenses before the light-sheet scanner, as shown in Fig. 2a. Ensure that the collimated laser beam is focused by the first lens onto the pivot galvo. The angular adjustment of the pivot scanner then results in a lateral shift of the collimated beam at the light-sheet scanner.

▲ **CRITICAL STEP** The beam diameter at the light-sheet galvo mirrors (X-galvo and Z-galvo) and their maximum apertures limit how far the collimated beam can be shifted by the pivot galvo without the beam being clipped. To avoid clipping the beam at the light-sheet galvos, ensure that the aperture of the light-sheet galvo is large enough to fully capture the laterally shifted beam introduced by the pivot galvo (lateral shift =  $\gamma_p f_{R2} = \beta f_\theta/M$ , Box 1). In our experience, imaging of the *Drosophila* and zebrafish embryos/larvae typically uses a pivot within the  $\pm 2^\circ$  angular range, so the aperture of the light-sheet galvo mirrors should be large enough to accommodate these angles. In addition, note that the numerical aperture (NA) of the light sheet in the sample plane can be adjusted by changing the focal length of the relay lenses around the pivot galvo, with all else in the

**Box 1 | Equations relating to light-sheet illumination parameters for the AutoPilot framework**

1 NA of the scanned light sheet in the sample plane:

$$\text{NA}_{\text{LS}} = \frac{M\emptyset_g}{2f_\theta}$$

2 Light-sheet full-width half-maximum (FWHM) thickness:

$$t_{\text{FWHM}} = \frac{\sqrt{2\ln 2}\lambda_{\text{ex}}}{\pi\text{NA}_{\text{LS}}}$$

3 Light-sheet length (practical field of view):

$$\Delta Y = \frac{2n\lambda_{\text{ex}}}{\pi\text{NA}_{\text{LS}}^2}$$

4 Optical angles of the light-sheet galvos to cover the respective  $\Delta X$  and  $\Delta Z$  fields in the sample plane:

$$\theta_{\Delta X} = \tan^{-1}\left(\frac{M}{f_\theta} \Delta X\right)$$

$$\theta_{\Delta Z} = \tan^{-1}\left(\frac{M}{f_\theta} \Delta Z\right)$$

5 Illumination light-sheet tilt ( $\alpha$ ) in the sample plane (Fig. 2d):

$$\alpha = \tan^{-1}\left(\frac{\delta z}{\Delta X}\right)$$

6 Illumination light-sheet pivot ( $\beta$ ) in the sample plane (Fig. 2e):

$$\beta = n_m \beta_m = \frac{\Delta z}{f_0}$$

7 Optical angle of the pivot galvo to generate a light-sheet pivot  $\beta$ :

$$\gamma_p = \frac{\beta f_\theta}{M f_{R2}}$$

**Definitions**

$f_0$  focal length of the objective

$f_{\text{TL}}$  focal length of the tube lens

$f_\theta$  focal length of the scan lens

$f_{R1}$  focal length of the lens before the pivot galvo

$f_{R2}$  focal length of the lens after the pivot galvo

$M$  magnification due to the objective and the tube lens, given by  $f_{\text{TL}}/f_0$

$\emptyset$  initial beam diameter

$\emptyset_g$  beam diameter at the light-sheet galvo,  $\emptyset_g = \emptyset f_{R2}/f_{R1}$

$\lambda_{\text{ex}}$  wavelength of the illumination beam

$\delta z$  Z offset in the sample plane across a field of  $\Delta X$  for a tilt of  $\alpha$

$\beta_m$  pivot angle in an immersion medium with refractive index  $n_m$

$\Delta z$  Z offset of the light-sheet in the back-focal plane of the objective due to the pivot galvo

system remaining the same. For a quicker setup, it is advisable to maintain the position of the pivot scanner and the second relay lens and choose the focal length of the first relay lens to obtain the desired illumination NA.

**Software integration of the adaptive imaging libraries** ● **Timing 2 d**

▲ **CRITICAL** In this section, we explain how to integrate the software library for adaptive light-sheet microscopy. When using a SiMView microscope design (see Steps 1–21 above), the LabVIEW-based microscope control software, including all adaptive imaging capabilities described in this protocol, can be obtained through an HHMI Material Transfer Agreement (contact P.J.K., kellerp@janelia.hhmi.org). If you wish to use and modify your own software for an existing light-sheet microscope (with up to two illumination arms and two detection arms), we provide instructions for this below.

**▲ CRITICAL** We assume that all the hardware is set up and ready: the optics are set up and aligned, and the mechano-optical actuators are installed and connected to the electronics.

**▲ CRITICAL** We strongly recommend reviewing the Supplementary Methods section of the original AutoPilot publication<sup>21</sup> to understand the theory behind spatiotemporal adaptive imaging. Importantly, the axis directions of all actuators (piezos and galvos) must follow the convention provided in this document.

**▲ CRITICAL** Depending on the programming framework used, we provide here three sets of instructions for integrating the AutoPilot core libraries into your own control software: Step 30 (for the Java module); Step 31 (for the C/C++ module); and Step 32 (for the LabVIEW module). These software integration steps (Steps 30–34) are not required when using the LabVIEW-based SiMVView microscope control software.

- 30 *Java integration.* The AutoPilot core library is primarily written in Java (JDK 8), which makes it straightforward to integrate into an existing Java project. We prepared a dedicated section discussing Java integration on the AutoPilot Wiki page: <https://github.com/MicroscopeAutoPilot/AutoPilot/wiki/javaapi>.
- 31 *C/C++ integration.* An overview of the application programming interface (API) and instructions are provided here: <https://github.com/MicroscopeAutoPilot/AutoPilot/wiki/ccppapi>. Documentation for the API can be found here: <https://github.com/MicroscopeAutoPilot/AutoPilot/blob/master/src/java/autopilot/interfaces/AutoPilotC.java>.
- 32 *LabVIEW integration.* C/C++ libraries can be integrated into LabVIEW projects in a straightforward manner by following the instructions here: <https://knowledge.ni.com/KnowledgeArticleDetails?id=KA00Z0000019Ls1SAE>.
- 33 Add a microscope state variable,  $S = (D_1, D_2, I_1, I_2, Y_1, Y_2, \alpha_1, \alpha_2, \beta_1, \beta_2, \dots)$ , to your control framework; the variable contains the current value of each DOF for each reference plane and for each color channel.
- 34 Add a correction variable,  $\Delta F = (\Delta F_{1,1}, \Delta F_{1,2}, \Delta F_{2,1}, \Delta F_{2,2}, \Delta Y_1, \Delta Y_2, \Delta \alpha_1, \Delta \alpha_2, \Delta \beta_1, \Delta \beta_2, \dots)$ , to your control framework; the correction variable will be populated with measurements reflecting the individual adjustments required to optimize each DOF. For example,  $\Delta F_{1,1}$  corresponds to the defocus measured between the first detection plane and the first light sheet, and  $\Delta Y_1$  corresponds to the translation along the illumination axis needed to optimize the position of the objective piezo for the first light sheet.

### Implementation of AutoPilot measurements ● Timing 3 d

**▲ CRITICAL** The algorithms described in this section relate to the five hardware modules that adjust different DOFs (see Steps 22–29 above and Fig. 2). It is possible to limit the AutoPilot framework to a subset of these modules (and to use different sets of DOFs in different experiments), but some modules require common mechanical or electronic adjustments to the microscope. Use Step 35 for software modules  $D$  and  $I$  (to control detection focus and light-sheet offsets respectively); use Step 36 for software modules  $\alpha$  and  $\beta$  (to control light-sheet angles  $\alpha$  and  $\beta$ , respectively); and Step 37 for software module  $Y$  (to control light-sheet focus  $Y$ ).

- 35 Use the following pseudocode for measuring  $D$  and  $I$  defocus for a given detection plane, light sheet, reference plane and color channel (light gray, comments; red, function names; green, numeric literals):

```
#Dependencies:
get_reference_plane_lightsheet_Z(...) # provided by host control software
get_reference_plane_detection_Z(...) # provided by host control software
get_reference_plane_lightsheet_Y(...) # provided by host control software
get_reference_plane_lightsheet_AB(...) # provided by host control software
set_lightsheet_Z(...) # provided by host control software
set_lightsheet_Y(...) # provided by host control software
set_lightsheet_AB(...) # provided by host control software
set_lasers_and_filters(...) # provided by host control software
set_detection_Z(...) # provided by host control software
acquire_image(...) # provided by host control software
dcts(...) # provided by AutoPilot core library
argmax(...) # provided by AutoPilot core library
```

```

#Input:
    Int      det_index,
    Int      ill_index,
    Int      color_index,
    Int      ref_plane_index,

    Float   radius,
    Int      nb_samples

#Output:
    Float   defocus
    Images  image_stack # for use to determine angles Alpha and Beta

def measure_DI:
    Zi          = get_reference_plane_lightsheet_Z(ref_plane_index)
    Zd_center   = get_reference_plane_detection_Z(ref_plane_index)
    Y           = get_reference_plane_lightsheet_Y(ref_plane_index)
    (A,B)       = get_reference_plane_lightsheet_AB(ref_plane_index)

    Zd_list = [-(nb_samples-1)/2, ... , 0 , ..., +(nb_samples-1)/2]
    Zd_list = radius*(2*Zd_list/(nb_samples-1))
    metric_list = []
    image_stack = []
    set_lightsheet_Z(Zi)
    set_lightsheet_Y(Y)
    set_lightsheet_AB(A,B)
    set_lasers_and_filters(color_index)

    for Zd in Zd_list:
        set_detection_Z(Zd_center+Zd)
        image = acquire_image(det_index, ill_index, color_index)
        image_stack.append(image)
        metric = dcts(image)
        metric_list.append(metric)

    defocus = argmax(Zi_list, metric_list)

```

- 36 Using the defocus stack `image_stack` acquired with the algorithm outlined above, compute the  $\alpha$  and  $\beta$  angles of the light sheet relative to the detection focal plane. The `stack_analysis` function from the AutoPilot core library is used for the computation. For a given detection plane, light sheet, reference plane and color channel, we can obtain the  $\alpha$  and  $\beta$  angles as shown below.

```

#Dependencies:
    stack_analysis(...) # provided by AutoPilot core Library
    getAlpha(...)        # provided by AutoPilot core Library
    getBeta(...)         # provided by AutoPilot core Library

#Input:
    Images image_stack # as obtained previously

#Output:
    Float alpha        # relative alpha angle between detection plane and Light sheet
    Float beta         # relative beta angle between detection plane and Light sheet

def measure_AlphaBeta:
    analysis_result = stack_analysis(image_stack)
    alpha = analysis_result.getAlpha()
    beta = analysis_result.getBeta()

```

- 37 Use the following pseudocode for measuring the Y correction for a given detection plane, light sheet, reference plane and color channel.

```

#Dependencies:
get_reference_plane_lightsheet_Z(...) # provided by host control software
get_reference_plane_detection_Z(...) # provided by host control software
get_reference_plane_lightsheet_Y(...) # provided by host control software
get_reference_plane_lightsheet_AB(...) # provided by host control software
set_lightsheet_Z(...) # provided by host control software
set_lightsheet_Y(...) # provided by host control software
set_lightsheet_AB(...) # provided by host control software
set_lasers_and_filters(...) # provided by host control software
set_detection_Z(...) # provided by host control software
acquire_image(...) # provided by host control software
dcts(...) # provided by AutoPilot core library
argmax(...) # provided by AutoPilot core library

#Input:
Int    det_index,
Int    ill_index,
Int    color_index,
Int    ref_plane_index,

Float  radius,
Int    nb_samples

#Output:
Float  bestY # measurement for Y

def measure_Y:
    Zi      = get_reference_plane_lightsheet_Z(ref_plane_index)
    Zd      = get_reference_plane_detection_Z(ref_plane_index)
    Y_center = get_reference_plane_lightsheet_Y(ref_plane_index)
    A,B     = get_reference_plane_lightsheet_AB(ref_plane_index)

    Y_list = [- (nb_samples-1)/2, ... , 0 , ..., +(nb_samples-1)/2]
    Y_list = radius*(2*Y_list/(nb_samples-1))
    metric_list = []
    image_stack = []
    set_detection_Z(Zd)
    set_lightsheet_Z(Zi)
    set_lightsheet_AB(A,B)
    set_lasers_and_filters(color_index)

    for Y in Y_list:
        set_lightsheet_Y(Y_center+Y)
        image = acquire_image(det_index, ill_index, color_index)
        image_stack.append(image)
        metric = dcts(image)
        metric_list.append(metric)

    bestY = argmax(Zi_list, metric_list)

```

#### Execution of AutoPilot measurements ● Timing 1 d

**▲ CRITICAL** In this section, we illustrate how to collect observations for all DOFs. For each color channel, reference plane and—when using a light-sheet microscope design with multiple illumination

and detection arms—also for each combination of detection and illumination arms, we collect the observations required to subsequently correct the microscope state. We also create a `missing_observations` vector to note which observations could not be obtained because of lack of image contrast or lack of fluorescence signal.

- 38 Collect observations for all DOFs and create the `missing_observations` vector:

```
#Dependencies:
measure_DI()          # defined above
measure_AlphaBeta()   # defined above
measure_Y()            # defined above
setDefocus()           # convenience function to set values in a observations vector
setAlphaBeta()          # convenience function to set values in a observations vector
setY()                 # convenience function to set values in a observations vector

#Input:
Int                  number_of_detection_arms    # number of detection arms
Int                  number_of_illumination_arms  # number of illumination arms
Int                  number_of_colors          # number of recorded colors
Int                  number_of_planes          # number of reference planes
Int                  number_of_samples_DI      # number of samples for DI
Int                  number_of_samples_Y       # number of samples for Y

Float                radius_DI              # radius for DI
Float                radius_Y               # radius for Y

#Output:
Vector<Float> observations      = [0, ... , 0]
Vector<Float> missing_observations = [false, ... , false]

def make_all_observations:

    for c in [0, number_of_colors[:]:
        for p in [0, number_of_planes[:]:
            for d in [0, number_of_detection_arms[:]:
                for i in [0, number_of_illumination_arms[::

                    (defocus, img_stack) = measure_DI(d,i,c,p,radius_DI,number_of_samples_DI)
                    (alpha, beta) = measure_AlphaBeta(img_stack)
                    bestY = measure_Y(d,i,c,p,radius_Y,number_of_samples_Y)

                    if defocus == 'missing':
                        missing_observations.setDefocus(d, i, c, p, true)
                    else
                        observations.setDefocus(d, i, c, p, defocus)

                    if defocus == 'missing':
                        missing_observations.setAlphaBeta(d, i, c, p, true)
                    else
                        observations.setAlphaBeta(d, i, c, p, alpha, beta)

                    if defocus == 'missing':
                        missing_observations.setY(d, i, c, p, true)
                    else
                        observations.setY(d, i, c, p, bestY)
```

### Implementation of state corrections ● Timing 1 d

- 39 Once measurements have been performed for all DOFs, compute the new state of the microscope, given the current state and observations, using the `qpsolve` function from the AutoPilot core library:

```

#Dependencies:
qpsolve() # defined in AutoPilot core Library

#Input:
Boolean      anchor_detection      # true -> detection DOF anchoring
Boolean      symmetric_anchor      # true -> symmetric anchoring
# false-> only first detection anchored
Int          number_of_colors      # number of recorded colors
Int          number_of_planes       # number of reference planes
Vector<Bool> sync_planes         # vector of sync plane indices.

Vector<Float> current_state       # current microscope's state
Vector<Float> observations        # current microscope's observations
Vector<Bool> missing_observations # true -> missing observation
Vector<Float> max_corrections     # max corrections for each DOF

#Output:
Vector<Float> new_state # new microscope's state

def correct_state:
    # the following function is provided in the core AutoPilot Library.
    new_state = qpsolve(anchor_detection,
                         symmetric_anchor,
                         number_of_colors,
                         number_of_planes,
                         sync_planes,
                         current_state,
                         observations,
                         missing_observations,
                         max_corrections)

```

### Software implementation of the microscope initialization procedure (Initial adaptation) ● Timing 1 d

- 40 Optimize the initial microscope state before the start of an imaging experiment, thus enabling the use of a system in a potentially unknown alignment state without compromising image quality. The following pseudocode illustrates how multiple successive rounds of observation and corrections with shrinking search radii can help to rapidly align a poorly aligned system.

```

#Dependencies:
make_all_observations() # defined above
correct_state()          # defined above

#Input:
Vector<Float> current_state
Int          number_of_rounds      # number of optimisation rounds
Int          number_of_detection_arms # number of detection arms
Int          number_of_illumination_arms # number of illumination arms
Int          number_of_colors       # number of recorded colors
Int          number_of_planes       # number of reference planes

Vector<Float> max_corrections     # max corrections for each DOF
Boolean      anchor_detection      # true -> detection DOF anchoring
Boolean      symmetric_anchor      # true -> symmetric anchoring
# false-> only first detection anchored
Vector<Bool> sync_planes         # vector of sync plane indices.

Int          number_of_samples_DI  # number of samples for DI
Int          number_of_samples_Y   # number of samples for Y
Float        radius_DI            # radius for DI
Float        radius_Y             # radius for Y

```

```
#Output:
none

def initial_adaptation:

    Vector<Float> working_state = current_state
    Vector<Float> observations
    Vector<Float> missing_observations

    for r in [0, number_of_rounds[

        (observations,missing_observations) =
            make_all_observations(number_of_detection_arms,
                                   number_of_colors,
                                   number_of_planes,
                                   number_of_samples_DI,
                                   number_of_samples_Y,
                                   radius_DI * 2^(-r),
                                   radius_Y * 2^(-r))

        correct_state(anchor_detection,
                      symmetric_anchor,
                      number_of_colors,
                      sync_planes,
                      current_state,
                      observations,
                      missing_observations,
                      max_corrections)
```

### Software implementation of the main image acquisition loop ● Timing 3 d

- 41 Use the following pseudocode to establish a basic image acquisition loop in a multicolor light-sheet microscope, including the steps needed for continuous microscope adaptation to the specimen.

```
#Dependencies:
acquire_stacks(...)                                # provided by host control software
wait_for_next_timepoint(...)                        # provided by host control software
collect_observations(...)                          # collects observation for a given
                                                # color, plane and DOF similar to
                                                # make_all_observations()

#Counter Syntax:
Counter[2,3,2] mycount = (0,0,0)
mycount+1 == (0,0,1)
mycount+2 == (0,1,0)
mycount+6 == (1,0,0)

#Input:
Int          nb_colors      # number of recorded colors
Int          nb_planes      # number of reference planes
Int          nb_obs         # number of observations

Boolean      anchor_detection # true -> detection DOF anchoring
Boolean      symmetric_anchor # true -> symmetric anchoring
                           # false-> only first detection anchored
Vector<Bool> sync_planes    # vector of sync plane indices.
Vector<Float> max_corrections # max corrections for each DOF

Object stack_acquisition_parameters # acquisition parameters
                                    # (exposure, nb planes, etc)
Float acquisition_period_seconds     # acquisition period in seconds
```

```

#Output:
none

def acquisition_loop:

    Counter[nb_colors, nb_planes, nb_det_arms, nb_ill_arms] counter = (0,0,0)
    Vector<Float> current_state
    Vector<Float> new_state
    Vector<Float> observations      = [0,      ... , 0      ]
    Vector<Float> missing_observations = [false, ... , false]

    for tp in [1, ... , nb_time_points]:

        acquire_stacks(stacks_acquisition_parameters)
        counter = counter+1

        if counter == (0,0,0):
            new_state = correct_state(anchor_detection,
                                         symmetric_anchor,
                                         nb_colors,

                                         nb_planes,
                                         sync_planes,
                                         current_state,
                                         observations,
                                         missing_observations,
                                         max_corrections)
            current_state = new_state

        (color, plane, dof) = counter
        collect_observations(color, plane, dof, observations, missing_observations)
        wait_for_next_timepoint(acquisition_period_seconds)

```

### Basic microscope alignment ● Timing 1 h

- 42 Basic alignment of the illumination path can be achieved by first establishing a conjugation of the light-sheet galvos to the objective's back-focal plane. To this end, first position the light-sheet galvos at the focal plane of the scan lens. Make sure that the distance between the scan lens and the tube lens is equal to the sum of their focal lengths. Next, explore the optimal position of the objective while scanning a galvo mirror that is to be made conjugate to the back-focal plane of the objective. The back-focal plane of the objective is conjugate to the galvo mirror when the light sheet in the front focal plane of the objective moves laterally without changing its angle. If using a dual-axis scanner as in SiMView, keep the distance between the two mirrors to a minimum and make the back-focal plane of the objective conjugate either to a position midway between the two galvo mirrors or to a galvo mirror that uses a larger tilt angle. Alternatively, both galvo mirrors can be made conjugate to the back-focal plane by adding a pair of relay lenses between them. While the light-sheet galvos are conjugated to the back-focal plane of the objective, conjugate the pivot galvo to the front focal plane of the objective. As such, the pivot galvo should be positioned at the focal plane of a pair of relay lenses before the light-sheet scanner (Fig. 2a). To ensure that the separation between each relay lens pair in the illumination path is accurate, a shear plate can be used as a guide to fine-tune the distance between them. Align the detection path such that the filter wheel is inserted into the infinity space situated between the detection objective and the tube lens. It is recommended that the detection path leading up to the camera be shielded from stray light using lens tubes.

**▲ CRITICAL STEP** For a successful AutoPilot imaging experiment, it is important that the microscope be roughly aligned—in the absence of a sample—before beginning the imaging. The focal planes of the detection objectives should be nearly identical, and the light sheets should be approximately coplanar with the detection focal planes (or, at the very least, within a distance that does not exceed the focus search radius used during AutoPilot initialization). If the ideal configuration is outside the search radius used during AutoPilot initialization, the AutoPilot may not converge on an optimal solution within the number of iterations allowed during the initialization procedure.

**Sample preparation for an adaptive light-sheet imaging experiment ● Timing 30 min**

▲ **CRITICAL** In this section, we will briefly discuss the sample preparation for a typical light-sheet microscopy experiment, using the example of the SiMView light-sheet microscope. The SiMView microscope has optical access to the sample from four directions, with two detection objectives and two illumination objectives orthogonal to the detection axis. The sample must be held securely on a four-axis mechanical stage that allows precise X, Y, Z and rotational positioning without any optical obstructions. In practice, the sample is typically embedded in a cylinder of low-concentration, low-melting-point agarose that has nearly the same refractive index as the aqueous medium that surrounds it. One limitation of agarose embedding is that it restricts changes in the shape of the sample. If the sample is expected to change its shape, it can be mounted inside a fluorinated ethylene propylene (FEP) tube that isolates it in a compatible environment and restricts its position to a very small range. We recommend using a custom-sized extruded FEP tubing manufactured by Zeus (product type Sub-Lite Wall) for this purpose; it has an i.d. of  $2,388 \pm 25 \mu\text{m}$ , a wall thickness of  $25 \pm 13 \mu\text{m}$  and a refractive index of 1.344. The following procedure is the typical method of embedding a sample in a cylinder of low-concentration agarose and is appropriate for *Drosophila* or zebrafish embryos, or, with a slight modification, isolated *Drosophila* nervous systems. The embedding procedure for a *Drosophila* embryo is visualized in Supplementary Video 1.

- 43 For zebrafish and *Drosophila* embryos and other similar embryos, prepare a 1% (wt/vol) solution of low-melting-point agarose in water (Reagent setup).  
▲ **CRITICAL STEP** In general, the low-melting-point agarose solution should be adapted to the sample and the agarose concentration should be kept as low as possible while ensuring mechanical support to the sample. The concentration can be adjusted to individual circumstances; lower concentrations can reduce mechanical constraints on the specimen and improve image quality by more closely matching the refractive index of the surrounding aqueous medium; higher concentrations, being more rigid, can decrease drift in the sample position during time-lapse recordings. We found that concentrations as low as 0.3% (wt/vol) still offer sufficient mechanical support to enable long-term imaging in a SiMView microscope. If mechanical constraints need to be eliminated altogether, it is also possible to use agarose-free sample preparation in FEP tubes<sup>43</sup>, as described above.
- 44 Maintain the liquid agarose at a temperature of 40–42 °C. This temperature provides a little working time in the subsequent embedding steps while minimizing heat stress to the sample.
- 45 Place a glass capillary tube into a cutoff pipette tip so that liquid agarose can be drawn into it.  
▲ **CRITICAL STEP** The inner diameter of the capillary should be matched to the size of the sample, providing enough space for a continuous cylinder of agarose around the sample to maintain mechanical stability while limiting the optical path length through the agarose. For *Drosophila* and zebrafish embryos, a 1.5-mm i.d. (2-mm o.d.) is optimal. Larger samples, such as zebrafish larvae, require a capillary with a 2.5-mm i.d. (3-mm o.d.).
- 46 Isolate the sample to be embedded. This may require dechorionation of embryos, dissection of a central nervous system or any sample preparation that maintains sample viability while increasing optical access to the sample by decreasing light scattering and refraction.
- 47 Transfer the sample in a small drop of liquid medium to an agarose-coated culture dish.
- 48 Flood the drop of liquid with 1 mL of liquid agarose.
- 49 Immediately draw the sample, surrounded by agarose, into the glass capillary. It is useful to fill the entire capillary with an unbroken volume of agarose, with the sample near the end of the capillary. Voids in the agarose can expand or contract during the recording, causing the sample to drift out of the field of view.
- 50 Use the points of fine forceps to swirl the agarose around the sample to position it in the center of the cylinder with an orientation that suits the imaging needs, typically with the long axis of the sample parallel to the long axis of the capillary.  
▲ **CRITICAL STEP** Continue to adjust the sample position until the agarose cools enough to form a gel. A 1% (wt/vol) agarose concentration will gel in a minute or two, whereas a higher concentration gels faster and lower concentrations can take much longer to form a gel.
- 51 After the agarose is fully gelled, push soft wax, such as dental wax or beeswax, into the end of the capillary opposite the sample location. This will push the sample outside of the glass and, thus, the illumination and detection axes will not pass through the glass.
- 52 Keep the sample submerged in medium as much as possible. Agarose exposed to air will quickly dehydrate and deform.

**Box 2 | AutoPilot high-speed imaging (HSI) setup**

**▲CRITICAL** This box describes instructions for setting up parameters for HSI-mode recordings (Fig. 4).

- The principles used to set up an HSI experiment are the same as those used for stage-mode recordings, with one distinct exception. In HSI mode, the reference planes (Step 55) are defined relative to the stationary sample position. For a *Drosophila* embryo with a diameter of 180 µm, typical reference planes would be -70, -50, -30, 0, 30, 50 and 70 µm. The imaging range is also set relative to the center position, in this case -100 to 100 µm.
- When the initial adaptation is performed, the HSI table will be filled in with the appropriate values. The Y adaptation mode (Steps 69–73) is not available with HSI because the piezoelectric positioners for the illumination objectives typically do not move quickly enough.
- Normally, adaptation during recording (Steps 56–59) is disabled in HSI experiments. If you anticipate that the sample will exhibit substantial changes in shape or optical properties, or that the microscope state will change substantially during the recording, imaging can be interrupted to perform adaptation by selecting ‘Preemptive adaptation’. Note that the regular interval between imaging time points will be disrupted.

Z Location (µm)	I1 (µm)	I2 (µm)	D1 (µm)	D2 (µm)	Sync Plane?
-70.00	-1.00	1.00	2.00	2.00	FALSE
-50.00	-2.03	1.65	2.00	2.00	FALSE
-30.00	-0.94	1.18	2.00	2.00	TRUE
0.00	-1.23	0.81	2.00	2.00	TRUE
30.00	-0.93	1.10	2.00	2.00	TRUE
50.00	-1.91	1.38	2.00	2.00	FALSE
70.00	-2.20	1.41	2.00	2.00	FALSE

Common D1 and D2 for Each Channel?

**Fig. 4 | Example interface for configuring reference planes in a high-speed recording.** A typical configuration of the high-speed imaging table (HSI table, as used in the SiMVview control software), showing the user-defined Z locations of the reference planes and sync planes and the AutoPilot-determined values for I and D at each of those planes (Box 2). The D and I values in the table are corrections applied after the detection objectives and the light sheets have moved to the defined reference planes. Above the table, the user can see the absolute D and I values for any selected reference plane.

### Sample mounting ● Timing 3–5 min

- 53 Place the embedded sample in the sample holder on the four-axis mechanical stage. Adjust the position of the stage to center the sample in the fields of view of both detection objectives and where it is approximately bisected by the focal plane of the detection objectives.

### Imaging mode configuration ● Timing 1 min

- 54 Select the recording mode. For example, a SiMVview light-sheet microscope has two distinct recording modes: in the first, stage mode, the sample is moved through stationary focal planes, and in the second, high-speed imaging (HSI) mode, the sample is held stationary and the focal planes and light sheets are moved through the sample. The AutoPilot can be used in both modes, but the setup procedures are slightly different. The stage mode is described in the main Procedure, and the modifications required for HSI are described in Box 2 (Fig. 4).

### Imaging volume and configuration of AutoPilot reference planes ● Timing 3–5 min

**▲CRITICAL** Reference plane setup. At each of these planes, the AutoPilot algorithm will assess the image quality and adjust the selected DOFs. At the imaging planes between (or outside) the reference planes, the AutoPilot will linearly interpolate between (or extrapolate from) neighboring reference planes and apply the appropriate corrections.

- 55 Specify the reference planes according to the guidelines in Box 3 (see also Fig. 5).

### Configuration of the main AutoPilot parameters ● Timing 1–2 min

**▲CRITICAL** This section describes the configuration of the main AutoPilot parameters, such as cooperative versus pre-emptive adaptation, time budget allocation, DOF scheduling and multiwavelength configuration. We discuss these parameters in the context of the AutoPilot integration

**Box 3 | Guidelines for specification of reference planes**

**▲ CRITICAL** Refer to these guidelines before setting up reference planes.

- The reference planes should span almost the entire Z dimension of the sample at approximately uniform intervals (Fig. 5). The first and last reference planes should be 10–20 µm from the surface of the sample. If a reference plane is too close to the surface of the sample, the search for optimal light-sheet offsets and angles may converge on a plane that has no information content, which may result in an incorrect alignment.
  - The distance between the first reference plane and its neighboring reference plane should also be small, e.g., 10–20 µm. Corrections between the first imaging plane, which is usually outside of the sample, and the first reference plane are extrapolated from the slope of corrections calculated for the first and second reference planes. Refraction caused by the first and last 20 µm of a curved sample such as a *Drosophila* or zebrafish embryo is very different from the refraction caused by the middle planes, where the light sheet enters the sample at angles approaching normal. To extrapolate accurately onto the first few planes, where the light sheet enters the sample at acute angles, the first two reference planes should be close to the front surface where the surface angle does not change markedly.
  - The remaining reference planes should be evenly spaced throughout the sample. We recommend a spacing on the order of 20–30 µm for *Drosophila* embryos and 150 µm for zebrafish embryos to ensure sufficiently precise sampling of the specimen's local optical properties. At least one plane near the center of the sample must have image information in both detection arms (Fig. 5c,d). That plane, designated a 'sync' plane, will be used to align the two detection objectives.
  - In stage mode, the first and last imaging planes are defined first. Then each of the reference planes is defined and one or more planes in the center are designated as sync planes. Each plane is defined as the absolute Z position of the mechanical sample stage.
  - In HSI mode, the reference planes are defined as detection objective positions relative to the fixed position of the sample stage (Box 2). The sync planes are chosen from planes that have image information in both detection arms. Last, the imaging Z range is defined as distances relative to the fixed position of the sample stage.
- ▲ CRITICAL STEP** For example, for a typical *Drosophila* embryo that is 180 µm in diameter, seven reference planes are placed at Z positions with the following distances from the front surface of the sample: 20, 40, 60, 90, 120, 140 and 160 µm, with sync planes at 60, 90 and 120 µm (Fig. 5c). For a 750-µm-diameter dechorionated zebrafish embryo, the reference planes are typically set at 25, 75, 225, 375, 525, 675 and 725 µm, with sync planes at 225, 375 and 525 µm (Fig. 5d).
- ▲ CRITICAL STEP** More reference planes can be used to obtain finer-grained adjustments to the microscope alignment, but this will require more time for both the initial adaptation and the periodic adaptation. It will also subject the sample to a larger laser energy load. Multiple sync planes will help ensure that the alignment of the two detection objectives will be based on images acquired from a plane that has reliable information in both detection arms. The position of the detection objectives will be determined by the last sync plane where the DCTS scores and image-quality metric curve fits reach the thresholds set by the user.

into the SiMView control software and provide a schematic overview of this user interface for parameter configuration in Fig. 6.

- 56 (Optional) 'Preemptive' and 'Stop Refocus if Too Long' modes are optional (Fig. 6a). If the interval between imaging time points is not long enough to produce any idle time, choose 'Preemptive' adaptation to interrupt the regular imaging intervals until the adaptation is complete. Alternatively, the adaptation can be stopped when reaching the next imaging time point by choosing 'Stop Refocus if Too Long'. The adaptation will continue at the same point during the next imaging interval. If neither option is chosen, adaptation will occur on schedule and will continue until the full adaptation routine is completed. This configuration may result in nonuniform time intervals between image acquisitions.
- 57 Select an adaptation mode (also referred to as 'Refocus Mode', Fig. 6a). '1 Plane' adapts a single reference plane at each adaptation step and minimizes the time devoted to each time point. 'N Planes/Channel' adapts a user-defined number of reference planes at each adaptation step, decreasing the number of adaptation intervals that are required for a complete update of the imaging parameters. Corrections are applied to the microscope alignment only after all the reference planes have been assessed for image quality, so electing to adapt half of the reference planes at each time point will cause updates to occur at every second time point. 'All Planes' will perform a complete adaptation and apply corrections at each adaptation interval. This option requires the most time and, depending on the time interval chosen for the time-lapse imaging experiment, can potentially subject the sample to a high energy load with its inherent photodamage.
- 58 Navigate to 'Planes per adaptation' when selecting the 'N Planes/Channel' option, to set the number of planes assessed at each adaptation step. A good strategy is to choose the number of planes that will fit into the wait time between the end of image acquisition and the subsequent imaging time point. This must be determined empirically, as the exact time required depends on the user-defined adaptation parameters, as well as the speed of the mechanical sample stages and the distance between the reference planes.

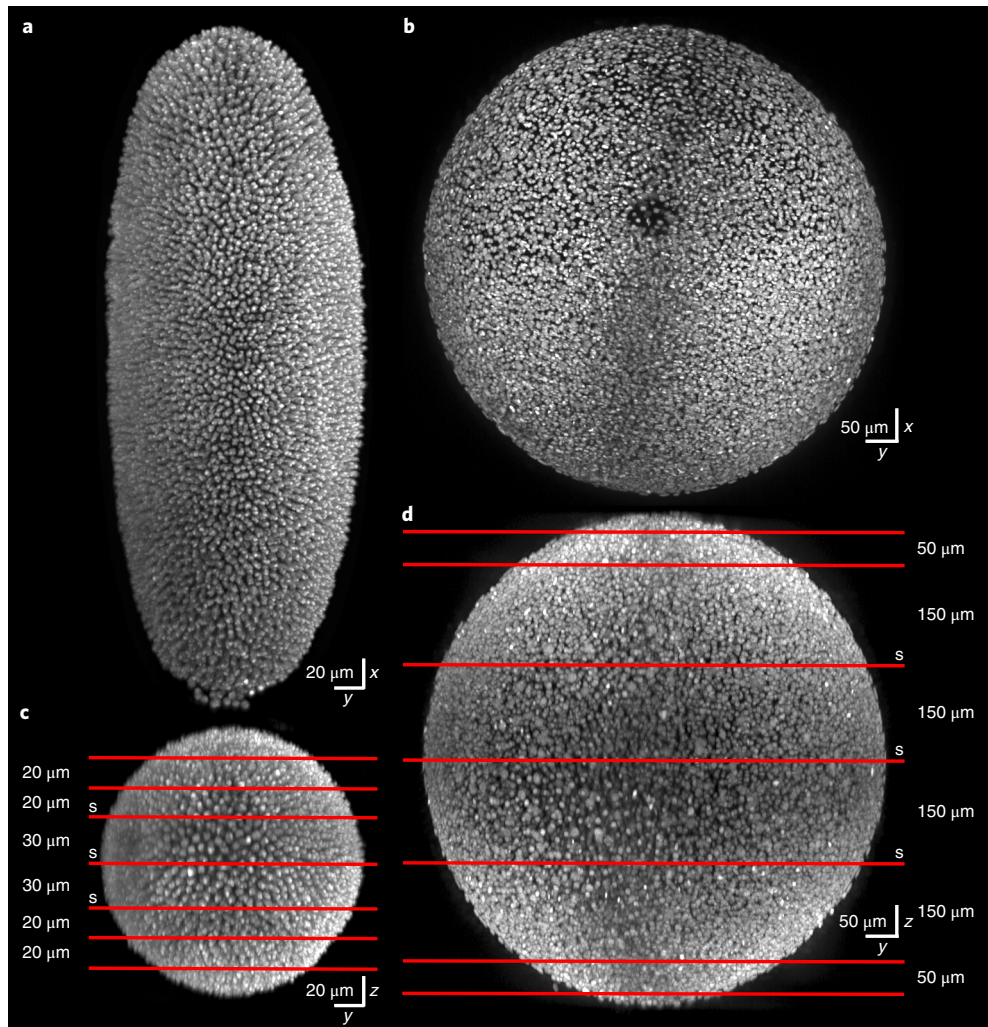


**Fig. 5 | Typical configuration of reference planes in fruit fly and zebrafish embryos.** **a-d,** Maximum-intensity projections of a *Drosophila* embryo at the blastoderm stage (**a,c**) and a zebrafish embryo at 90% epiboly (**b,d**). The x-y projections (**a,b**) represent the view of the specimen as seen along the detection axis. The y-z projections (**c,d**) show a view of the specimen from above. The red lines in the y-z projections indicate the z planes that were chosen as reference planes. The z planes labeled with an 's' are the sync planes. Scale bars, 20  $\mu\text{m}$  (**a,c**); 50  $\mu\text{m}$  (**b,d**).

59 Choose ‘Enable Master Wavelength’ (Fig. 6a) for a multicolor recording, when you prefer to assess image quality using a single laser wavelength, and apply the correction to all the active color channels. This reduces the time required to completely adjust the microscope but may produce suboptimal results in the dependent wavelengths, for which refraction and chromatic aberrations in excitation and emission light paths could be substantially different. In certain types of multicolor experiments, in which expression of one fluorophore begins late in the time-lapse recording, it can be beneficial to select a master wavelength that is appropriate for a ubiquitously expressed label that is present throughout the recording. In that case, when label expression begins in a dependent wavelength, the adjustments are already approximately correct.

**▲ CRITICAL STEP** Alternative strategies may produce better results in multicolor recordings. The AutoPilot algorithm is sufficiently robust to return reliable results on very weak signals, as it does not rely on signal intensity. In practice, it can reliably adapt the microscope using green autofluorescence in the *Drosophila* embryo. If it is set up to adjust quickly, by selecting the ‘All Planes adaptation mode’ or perhaps choosing to adapt half of the planes at each time point, the AutoPilot framework will adjust to new labels very soon after they appear, provided that the optimal alignments are within the search radius. Alternatively, the master wavelength can be used for the initial adaptation and turned off for the adaptation during image acquisition. This ensures that the starting values for the dependent wavelengths are close to the optimal values and increases the chances that the adaptation will quickly find a good solution when label expression begins.

**a**

AutoPilot Basic Setup

Enable AutoPilot?

Preemptive?

Stop Refocus if Too Long?

Refocus Mode N Planes/Channel

Planes per Refocus 4

Enable Master Wavelength?

Master Channel (nm) 488

Laser Power Factor 1.00

Focus Type D

Initialize?  Refocus?

Initialize Start Radius 40.00

Initialize End Radius 10.00

Initialize Iterations 3

Refocus Radius 10.00

Refocus Interval 1

Initialize Sampling 11

Refocus Sampling 11

First Settle (ms) 30

Settle (ms) 5

Cleanup I?

Sampling Cleanup I 11

Radius Cleanup I 20.00

**b**

Focus Type  $\alpha, \beta$

Initialize?  Refocus?

Initialize Start Radius 20.00

Initialize End Radius 20.00

Initialize Iterations 1

Refocus Radius 20.00

Refocus Interval 1

Initialize Sampling 11

Refocus Sampling 11

First Settle (ms) 30

Settle (ms) 5

Cleanup I?

**c**

AutoPilot Advanced Setup

Anchor Detection DOF?

Symmetric Anchoring?

Correction Dampening?

Log Diagnostics?

Log Images?

Progressive Updates?

Use Structured Illumination?

Get Angles from D Stack?

Camera 1 Orientation Standard

Camera 2 Orientation Standard

$\alpha$  Smoothing Median

$\beta$  Smoothing None

Y Smoothing Parabola

Angles Min Fit Probability 0.96

Dampening Radius ( $\mu\text{m}$ ) 0.00

Max D Correction ( $\mu\text{m}$ ) 2.00

Max I Correction ( $\mu\text{m}$ ) 0.10

Max Y Correction ( $\mu\text{m}$ ) 100.00

Max  $\alpha/\beta$  Correction ( $^\circ$ ) 0.20

PSF Support Diameter (px) 3.00

Min Fit Probability 0.80

Min DCTS Value 7.80E-5

Number of  $\beta$  Offsets 4

$\beta$  Offsets -1.0  -2.0  1.0  2.0

**Fig. 6 | Example interface for configuration of AutoPilot parameters.** **a-c**, Typical settings for a stage-mode recording with the AutoPilot basic setup for  $D/I$ ,  $Y$ ,  $\alpha$  and  $\beta$  adaptation (**a,b**; Steps 60–75) along with a typical AutoPilot advanced setup (**c**; Steps 76–86).

### Configuration of AutoPilot DOFs ● Timing 1–3 min

▲ **CRITICAL** This section describes how to set up AutoPilot parameters for adaptation of all DOFs:  $D$ ,  $I$ ,  $Y$ ,  $\alpha$  and  $\beta$  (Fig. 6a,b).

- 60 *Adaptation type D (Steps 60–69)*. Use adaptation type  $D$  (also referred to as ‘Focus Type  $D$ ’) to find the optimal positions of the detection objectives ( $D$ ) and the optimal light-sheet offsets at each reference plane ( $I$ ) (Fig. 6a, central box). Determine whether the  $D$ -type DOF should be used for initial adaptation, during the recording or both. Initial adaptation iteratively measures image quality and adjusts alignment before imaging begins. The user defines the number of iterations and the starting and ending search radii. If selected, the AutoPilot can periodically perform one round of  $D$ -type adaptation at user-defined intervals during a time-lapse recording.
- 61 Set the search radius for the first round (‘Initialize Start Radius’) and the last round (‘Initialize End Radius’) of the initial adaptation. This search radius applies to both the detection objective positions ( $D$ ) and the light-sheet offsets ( $I$ ). The start radius must be large enough to encompass any misalignments of the microscope and the end radius should be small enough to provide sufficiently precise values for the  $D$  and  $I$  positions. Typical values for most samples are ‘Initialize Start Radius’ equal to 40  $\mu\text{m}$  and ‘Initialize End Radius’ equal to 10  $\mu\text{m}$ . A smaller end radius is not recommended, as a reduced range may not be adequate to produce a smooth focus-quality curve with a recognizable peak that can be precisely fit by a Gaussian function.
- 62 Set the number of iterations for the initial adaptation. The first iteration will use the starting search radius and the last iteration will use the ending search radius. As the search radius decreases, the AutoPilot framework will apply corrections from the previous iterations and explore a smaller range of  $D$  and  $I$  positions and return a more precise solution. Typically, three iterations are used to span the range between a start radius of 40  $\mu\text{m}$  and an end radius of 10  $\mu\text{m}$ .
- 63 Ensure that the search radius is never so small that there is not enough variation in the DCTS image-quality metric to produce an approximately Gaussian curve. A curve will be fitted to the

values, and the peak of the curve will be used as the optimal  $D$  or  $I$  position. If the range is too small, it may not be possible to closely fit a Gaussian curve, and the curve will be disregarded. The image-quality metric curves, the fitted Gaussian curve and the best offset values are displayed on the ‘Autofocus Main Display’. In addition, there are displays of the values of the DCTS score, the fit probability and a binary indication of whether both these values are above user-defined thresholds. When the calculated values supersede the thresholds, the best  $D$  and  $I$  values are used to apply corrections. For *Drosophila* and zebrafish embryos, *Drosophila* and zebrafish brains, and many other samples, a radius of 10  $\mu\text{m}$  is the minimum value to reliably create a usable curve.

- 64 Set ‘Refocus Radius’ to determine the range of offsets that will be explored when adapting during the recording. In this case also, the range of the search should be large enough to produce an image-quality metric curve with a distinct peak. If a Gaussian curve cannot be fit to the metric values, the adaptation will be ignored, and no corrections will be applied to the microscope for that reference plane. A range of 10  $\mu\text{m}$  is typical for most samples.
- 65 Set the ‘Refocus Interval’, which is the number of imaging time points between adaptation rounds during recording. An interval of 1 will adapt after every time point, which will result in faster adjustments of the microscope to changing conditions but will also subject the sample to the maximum amount of light. With many adaptation iterations, the reference planes can be subjected to a large amount of light, which can cause bleaching and photodamage in those regions of the sample. To reduce this effect without sacrificing the temporal or spatial resolution, the laser power factor can be decreased to reduce the laser power used during all AutoPilot activity. Typically, values of 0.90 or 0.85 (90% and 85%) save a substantial amount of light without adversely affecting the AutoPilot results. Additional mechanisms for further reducing energy load are described in the ‘AutoPilot advanced setup’ section below (see in particular Step 81, which allows reduction of energy load by a factor of 2 through the use of structured illumination).
- ▲ **CRITICAL STEP** The optimal adaptation interval depends on the nature of the sample being imaged. For a long time-lapse recording of a developing embryo, the interval between image acquisition time points is typically 30 s–5 min. During those types of recordings, in which the shape or content of the sample is likely to change between time points, a complete adaptation and parameter update should be performed frequently, e.g., at every time point or every second time point. If there is not sufficient wait time between image acquisitions, the adaptation can be spread across two time points by specifying that half of the planes are assessed at each adaptation step during the recording. For HSI, the interval between time points is too brief for adaptation during recording (Box 2). Usually, high-speed recordings are so short that the sample does not change enough to warrant adaptation. If adaptation is necessary, the high-speed recording can be interrupted by selecting ‘Preemptive’ adaptation and specifying a large interval of time points between adaptation steps, e.g., 1,000 time points in a typical zebrafish whole-brain functional imaging experiment performed at 2–4 Hz. Note that the regular time intervals between images will be discontinuous.
- 66 Set the number of samples used for initial adaptation as well as for adaptation during recording. The number of samples is the number of different light-sheet offsets evaluated at each reference plane. The samples are uniformly distributed across the search radius and determine the precision of the AutoPilot solutions. The number of samples is used in conjunction with the search radius to construct the image-quality metric curves, so there must be enough samples to construct a usable curve. A minimum of 11 samples is usually adequate for search radii of  $\geq 10 \mu\text{m}$ .
- 67 Select the ‘First Settle (ms)’ and ‘Settle (ms)’ options to add a little wait time after the detection objectives move to a new reference plane or after the detection objectives move to a new position within the search range at a reference plane, respectively. These settle times allow the piezoelectric positioners time to stabilize. The optimal settling times are dependent on the properties of the individual positioners and are best determined empirically.
- 68 (Optional) Use ‘Cleanup I’ to provide one additional round of adaptation for DOF  $I$ . This round of adaptation is useful after angle corrections are applied when the axis of rotation of the light sheet produced by the pivot galvos is not at the center of the field of view. In that case, any adjustment of the angles will also produce an offset that must be corrected with ‘Cleanup I’. ‘Cleanup I’ is typically not used after  $D$ -type adaptation.
- 69 *Adaptation type Y (Steps 69–73)*. Use adaptation type Y (also referred to as ‘Focus Type Y’, Fig. 6b, right) to find the optimal positions of the illumination objectives and, thus, the optimal locations of the light-sheet waist along the illumination axis. When setting up the microscope for bidirectional illumination, these locations are typically manually shifted away from the center of the field of view

toward the source of the light sheet by a quarter of the width of the sample. That puts the waist of the left light sheet in the center of the left half of the sample and the waist of the right light sheet in the center of the right half of the sample. For example, for an ~200- $\mu\text{m}$ -wide *Drosophila* embryo, the waist offsets are typically manually set to a distance of 50  $\mu\text{m}$  from the center of the field of view during microscope setup. For a 600- $\mu\text{m}$ -wide zebrafish embryo, the offsets are typically 150  $\mu\text{m}$  away from the center of the field of view.

- 70 Determine whether the Y-type adaptation should be used initially, during the recording or both. During both the initial adaptation and during the recording, the Y adaptation occurs after all iterations of the D adaptations are complete. However, for typical search radii, the Y adaptation takes too long to use during the recording. Y adaptation is therefore usually used only for the initial adaptation.
- 71 Set the Y search radii. Ideally, the range of illumination objective positions explored would cover the half of the sample closest to the source of the light sheet. In a sample with a circular cross-section, such as a *Drosophila* or zebrafish embryo, the waist of the light sheet should be close to the center of the image when images are acquired from planes close to the detection objectives, where all the content is near the middle of the image. For planes near the center of the embryo, where high-contrast image content may be near the edges of the image, the waist of the light sheet should be close to the edge of the image as well. To accomplish that, the illumination objectives must move a distance equivalent to half the diameter of the sample. For a *Drosophila* embryo with a diameter of 180  $\mu\text{m}$ , a Y search radius of 100  $\mu\text{m}$  is more than large enough to track the useful content throughout the sample. For a zebrafish embryo with a diameter of 600  $\mu\text{m}$ , the Y search radius should be at least 200  $\mu\text{m}$ . In some cases, the Y search range may be limited by the range of motion of the illumination objective positioner.
- 72 Set the number of samples. The Y adaptation typically uses one iteration with the same start radius and end radius. The number of samples should be large enough to produce a smooth image-quality metric curve. For a search radius of 100  $\mu\text{m}$ , 21 samples will produce a smooth curve. If the search radius is large enough and the number of samples is adequate, the AutoPilot main display will show a smooth curve with a single peak. If no peak is displayed, the search range was probably not big enough to find the edge of the sample.
- 73 Use ‘Cleanup I’ to adjust the I offsets after Y has been adjusted. If the illumination objectives are aligned to be co-axial with their piezoelectric positioners, changes in Y position will not introduce an offset to the light sheet. If there is any misalignment, ‘Cleanup I’ will correct any introduced offset errors.
- 74 *Adaptation type  $\alpha$  and  $\beta$  (Steps 74 and 75).* Use adaptation type  $\alpha$  and  $\beta$  (also referred to as ‘Focus Type  $\alpha$ ,  $\beta$ ’, Fig. 6b, left) to calculate light-sheet angles  $\alpha$  and  $\beta$  relative to the detection focal plane from a defocus stack (see also Step 36). At each reference plane, the detection objectives are moved through the search range, the images are divided into tiles and the image quality is measured for each tile. Because  $\alpha$  and  $\beta$  adaptation is typically performed after D-type adaptation, it is sufficient to search within a small radius of objective positions, e.g., 20  $\mu\text{m}$ . The computation of  $\alpha$  from the defocus stack is usually sufficiently precise to directly determine the optimal setting of this parameter. As changes in  $\beta$  typically have a more pronounced impact on the illumination light path, an iterative scheme can be used to increase the robustness of the  $\beta$ -angle calculation and correction. For this purpose, the pivot galvos are used to introduce  $\beta$  angles to the light sheet and the image quality is measured again. This is repeated for a user-defined number of  $\beta$ -angle offsets. Because the angle calculations are repeated several times with different angle offsets, it is sufficient to perform just a single iteration of  $\alpha$  and  $\beta$  adaptation using the same start radius and end radius. The  $\alpha$  and  $\beta$  adaptation occurs after the Y adaptation is complete, if the Y adaptation is activated. If Y adaptation is not activated,  $\alpha$  and  $\beta$  adaptation occurs after all iterations of the D adaptation are complete.
- 75 **▲ CRITICAL STEP** When using the SiMView control software, ‘Get Angles from D Stack’ must be activated to use this feature (Fig. 6c). There is no graphical output from the  $\alpha$ - and  $\beta$ -adaptation procedure, aside from a small pop-up window that indicates that the angle calculations are taking place. After the calculations are complete, corrections are made to the  $\alpha$  and  $\beta$  angles by adjusting the movements of the pivot galvos.
- 75 Activate ‘Cleanup I’ for  $\alpha$  and  $\beta$  adaptation. It is probable that the axis of rotation of the light sheet produced by changes in the pivot galvo is not at the exact center of the field of view (or at the position of the light-sheet waist). In this situation, if a  $\beta$ -angle correction is applied, it will necessarily apply a light-sheet offset. ‘Cleanup I’ will correct this offset.

▲ **CRITICAL STEP** Angle calculations take more time than *D*-type adaptations.  $\alpha$  and  $\beta$  adaptation is usually useful only if you expect the sample to change its shape or composition during the recording, which may independently change refraction effects at the location of each reference plane. Typically,  $\alpha$  and  $\beta$  adaptation is performed at intervals that are warranted by the changing morphology of the sample, which are much less frequent than *D*-type adaptation. In developing *Drosophila* or zebrafish embryos, the *D*-type adaptation is performed every one or two time points, whereas the  $\alpha$  and  $\beta$  adaptation is performed every 100 time points. Be aware that *D*-type adaptation takes priority over every other type of adaptation. If *D*-type adaptation and  $\alpha$  and  $\beta$  adaptation are scheduled for the same time point,  $\alpha$  and  $\beta$  adaptation will not begin until *D*-type adaptation has been completed for the specified number of planes. If the ‘Stop Refocus if Too Long’ option is chosen,  $\alpha$  and  $\beta$  adaptation may not be completed for the specified number of planes during that interval. The  $\alpha$  and  $\beta$  adaptation will not continue until the next scheduled  $\alpha$  and  $\beta$  adaptation step, which in this example is 100 time points later. If it is important to complete the  $\alpha$  and  $\beta$  adaptation on time, deselect ‘Stop Refocus if Too Long’. The *D*-type adaptation and  $\alpha$  and  $\beta$  adaptation will occur on schedule, but the time interval between imaging time points will not be uniform.

### AutoPilot advanced setup ● Timing 1–2 min

▲ **CRITICAL** This section describes instructions for setting up AutoPilot’s advanced parameters (Fig. 6c). We recommend going through these parameters at least once to make sure that the configuration indeed reflects the intended operation of the AutoPilot framework. After this initial setup, a fixed set of parameters can typically be used for most, if not all, experiments performed with the microscope.

- 76 Select the ‘Anchor Detection DOF’ option to make the AutoPilot determine the alignment of the two detection objectives at the sync plane and apply those values to all the planes in the sample. The less useful alternative is for the detection objective positions to change at every plane.
- 77 Select the ‘Symmetric Anchoring’ option in order to move both detection objectives equally to correct for misalignment at the sync plane. The less useful alternative holds the first detection objective (D1) stationary and moves the second detection objective (D2) to match. The danger of this option is that the second detection objective may move so far that it disrupts the watertight seals and causes the sample chamber to leak.
- 78 Select the ‘Correction Dampening’ option to limit the maximum correction applied at any single adaptation step to the values that the user specifies in ‘Max D Correction’, ‘Max I Correction’, ‘Max Y Correction’ and ‘Max  $\alpha/\beta$  Correction’.
- 79 Select the ‘Log Images’ and ‘Log Diagnostic’ options to save images acquired during adaptation and a text file recording the focus metrics calculated at each adaptation. These logs are helpful for troubleshooting.  
? TROUBLESHOOTING
- 80 Select the ‘Progressive Updates’ option to apply corrections to planes individually as the reference planes are assessed during recording adaptation. If half of the reference planes are evaluated during an adaptation step, the resulting corrections are applied before the next imaging time point. If there is a correction to the position of the detection objective, this can disrupt the geometrical continuity of the image samples, with effective Z-steps at the center of the sample smaller or larger than the rest of the Z-steps. The preferred alternative is to not use progressive updates and, instead, apply corrections to the entire image stack after the full round of in-experiment adaptations has been completed.
- 81 Select the ‘Structured Illumination’ option to increase contrast in low-contrast samples and improve the performance of the DCTS image-quality metric. Structured illumination furthermore reduces the laser light energy load by a factor of 2.
- 82 Select ‘Get Angles from D Stack’ to adjust light-sheet angles. This option is used in conjunction with  $\alpha$  and  $\beta$  adaptation. Failure to select ‘Get Angles from D Stack’ will result in failure of the angle assessment.
- 83 Select the ‘Angles Min Fit Probability’ parameter to define a minimal probability threshold for the fitting of light-sheet angles  $\alpha$  and  $\beta$  in defocus image stacks. This is useful to prevent fitting parameters that are noisy and thus not informative.
- 84 Select the ‘Min Fit Probability’ parameter to define a minimal probability threshold for the image-quality metric curve fitting. As above, this helps prevent erroneous fitting.
- 85 Select the ‘Min DCTS Value’ parameter to define a minimum DCTS threshold for the image-quality metric curve fitting. As above, this helps prevent erroneous fitting.
- 86 Select the ‘Beta Offsets’ parameter to set the number of different  $\beta$  angles that will be explored while determining the best light-sheet angles during initial adaptation and during recording. The  $\beta$  angles to be used are specified in the  $\beta$ -offset window.

**Configuration of time-lapse imaging** ● **Timing** 3–5 min

**▲ CRITICAL** To start the image acquisition process using the SiMView microscope control framework, the following parameters must be configured.

- 87 *Laser power*. Equalize laser power in the two illumination arms by imaging a single reference plane and comparing signal intensities when illuminated individually by both light sheets. Adjust the power of both illumination arms such that they produce approximately the same signal intensities. Equalization works best after the initial focus has optimized the light-sheet offsets.
- 88 *Acquisition interval*. The interval must be long enough to acquire all images and include sufficient time for AutoPilot measurements at the number of reference planes the user has chosen to be assessed at each time point. In certain types of experiments with sensitive specimens, it can furthermore be beneficial to include some idle time (during which the lasers will be off) during each interval to provide the cells a chance to recover from oxidative photodamage and thereby maximize sample viability. If the interval is set to a shorter time than the time required to acquire the specified images, image acquisition will be continuous, and time intervals may vary depending on the exact amount of time spent on data acquisition for each time point.
- 89 *Duration of recording*. Set the duration of the time-lapse recording.
- 90 *Data folder*. Enter the path name of the root folder you would like to use to store the data for all experiments performed in the current imaging session.
- 91 *Experiment identifier*. Enter a text string that will identify the recording. The SiMView software will append a time stamp to the file name and use this string as the name of the subfolder that will contain the image data and log files acquired in the current experiment.
- 92 *Data structure and file format*. Enable image logging and select a file format. There are several choices that depend on the type of recording. Slow developmental recordings are commonly written to the hard drive in a structured format in which TIFF images from each time point are stored in a separate folder. High-speed functional recordings are commonly written to the hard drive in an unstructured format in which raw binary files from all time points are stored within a single folder. The unstructured stacks can be read with Fiji by opening the raw data file and specifying the size of the spatial dimensions of the image stack.
- 93 *Control mode*. Put the microscope into ‘Experiment Mode’ and click on ‘Start Acquisition’. Progress bars will indicate the progress through the experiment.

## Troubleshooting

Troubleshooting advice can be found in Table 7.

**Table 7 | Troubleshooting table**

Problem	Possible solutions
Suboptimal image quality/ AutoPilot failure	<p>The most likely cause of AutoPilot failure is use of search ranges that are not large enough to include the optimal objective positions or light-sheet parameters. The ranges can be increased, with the consequence of increasing the time required for adaptation, if the number of samples is also increased, or decreasing the resolution of the adaptation parameters, if the number of samples is not increased</p> <p>The most conservative way to ensure that the AutoPilot returns good results and makes appropriate corrections to the microscope is to start with a well-aligned microscope and to check that the initial adaptation produces good image-quality metric curves and good images before the recording begins. After the initial adaptation, check the image quality at every reference plane and every color, adjust as necessary and save the new objective positions, light-sheet offsets and light-sheet angles for each reference plane. It is best to check and adjust the image quality for each light sheet independently. The user can double-check and fine-tune the manual corrections by running a single iteration of the initial adaptation and inspecting each image-quality curve as it is produced</p> <p>When using the SiMView control software for AutoPilot control and observing suboptimal image quality, there are several options for diagnosing AutoPilot problems. When the AutoPilot is being configured, the user can elect to ‘Log Diagnostics’ (Fig. 6c), which saves a text file with objective positions, light-sheet offsets and angles for each reference plane at each time point; the DCTS scores and Gaussian fit probabilities for each reference plane at each adaptation step; and the corrections applied to the microscope throughout the recording. The user can also elect to ‘Log Images’ (Fig. 6c), which saves every image sequence for each reference plane at each adaptation step. These two logs can be inspected post hoc to determine where, when and why the AutoPilot failed. A detailed description of the logs and strategies for utilizing them for diagnosing problems with the initial AutoPilot setup or the AutoPilot configuration in a specific experiment are provided in the ‘Anticipated results’ section</p>

## Timing

When following the instructions provided here, building the adaptive SiMView light-sheet microscope should take on the order of 1 week, once all commercial and custom microscope components have been delivered and/or manufactured (Steps 1–21). Long lead times of up to 4 months for certain microscope components are typically the main cause for delays in microscope development. As briefly discussed in the ‘Experimental design’ section above, the items with the longest lead times for the SiMView microscope will usually be the optical table, laser system, custom f-theta lens, motorized stages, piezo positioners, galvanometer scanners and cameras. The lead time for fabrication of custom mechanical components can vary from a few weeks to several months, depending on the vendor and its workshop’s current workload. When integrating AutoPilot hardware modules into an existing microscope, the items with the longest lead times will usually be the piezo positioners, galvanometer scanners and potentially some of the custom mechanical parts. We thus strongly recommend ordering parts as early as possible to avoid delays.

Integration of the AutoPilot core libraries into an existing microscope design can take ~2–4 weeks, depending on the complexity of the host control software and the experience and skill set of the software engineer. Alternatively, installation, configuration and testing of the SiMView control software (which includes the AutoPilot framework) takes ~1 week.

Basic alignment of the microscope should be performed well before sample preparation to avoid delays once the sample is ready. We recommend reserving ~1 h for microscope alignment. Sample preparation and mounting takes ~30 min. Finally, setting up the AutoPilot framework and time-lapse imaging parameters for a new specimen takes typically between 5 and 30 min, depending on the complexity of the imaging experiment (the relevant factors include, e.g., the size of the specimen and the corresponding number of reference planes, the number of DOFs of the AutoPilot framework enabled in the experiment, the number of color channels, the imaging of multiple targets in the sample chamber and the use of multiview imaging based on sample rotation).

Steps 1–21, implementation of the light-sheet microscope: 1–2 weeks

Steps 22 and 23, hardware module *D*: 2 d

Steps 24 and 25, hardware module *Y*: 2 d

Steps 26 and 27, hardware module *I*: 2 d

Step 28, hardware module  $\alpha$ : none

Step 29, hardware module  $\beta$ : 2 d

Steps 30–34, software integration of the adaptive imaging libraries: 2 d

Steps 35–37, implementation of AutoPilot measurements: 3 d

Step 38, execution of AutoPilot measurements: 1 d

Step 39, implementation of state corrections: 1 d

Step 40, software implementation of the microscope initialization procedure (initial adaptation): 1 d

Step 41, software implementation of the main image acquisition loop: 3 d

Step 42, basic microscope alignment: 1 h

Steps 43–52, sample preparation for an adaptive light-sheet imaging experiment: 30 min

Step 53, sample mounting: 3–5 min

Step 54, imaging mode configuration: 1 min

Step 55, imaging volume and configuration of AutoPilot reference planes: 3–5 min

Steps 56–59, configuration of AutoPilot main parameters: 1–2 min

Steps 60–75, configuration of AutoPilot DOFs: 1–3 min

Steps 76–86, AutoPilot advanced setup: 1–2 min

Steps 87–93, configuration of time-lapse imaging: 3–5 min

## Anticipated results

The successful implementation of the protocols described here yields a light-sheet imaging framework capable of (fully or at least partially) recovering diffraction-limited resolution and improving signal strength in multicellular biological specimens whose optical properties would otherwise degrade image quality by disrupting spatial overlap of light sheets and detection focal planes. Substantial improvements in image quality are typically observed, e.g., in zebrafish and *Drosophila* embryos (Fig. 7), in particular when conducting long-term, time-lapse imaging, as well as in the zebrafish larval brain and in nervous system explants extracted from *Drosophila* larvae.

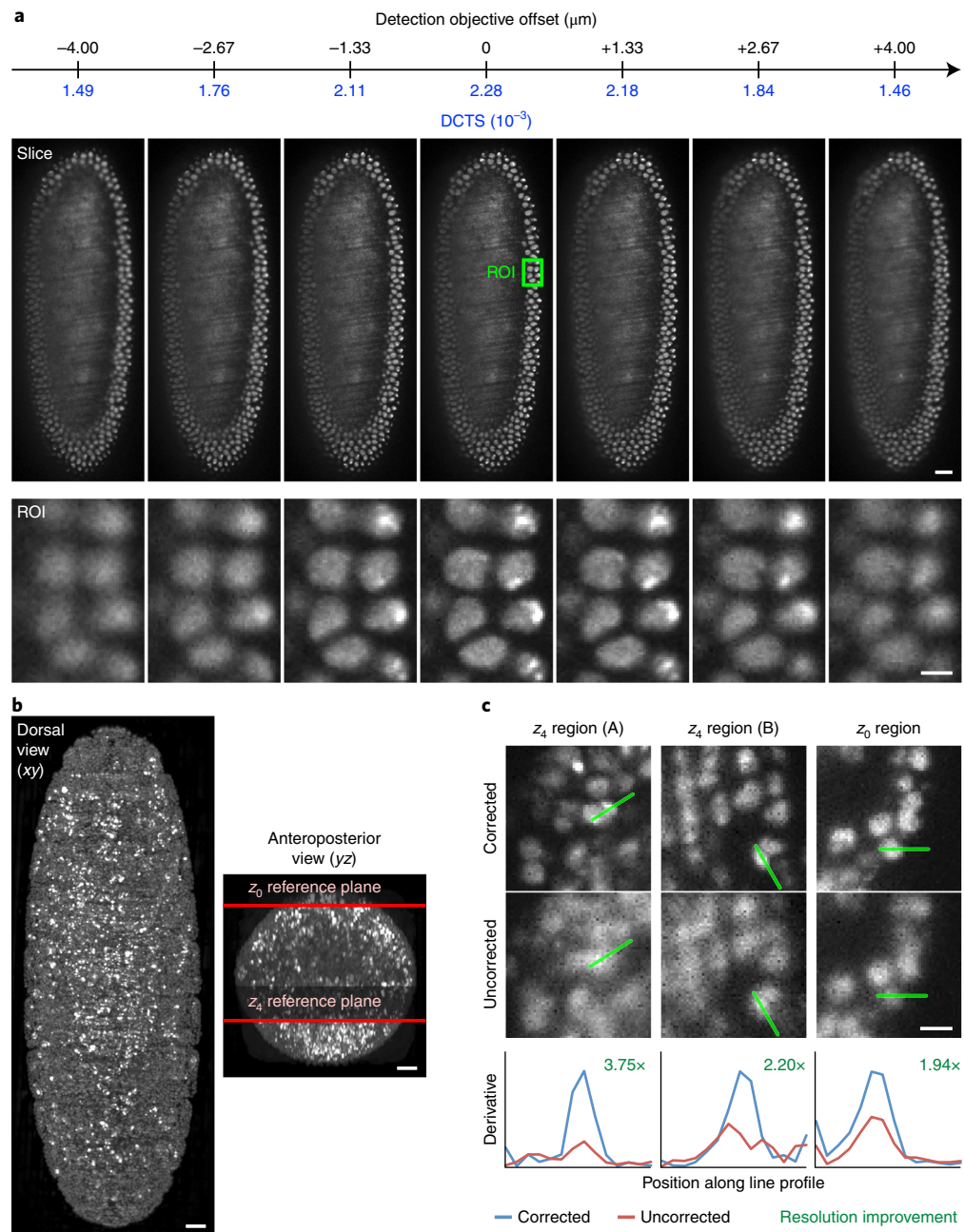


**Fig. 7 | Defocus measurements and optimization of resolution with the AutoPilot framework.** **a**, Sequence of image-based defocus measurements in a blastoderm-stage *Drosophila* embryo expressing a nuclear-localized fluorescent marker. The AutoPilot framework acquired seven images while varying the position of the detection objective relative to the stationary light sheet (entering the sample from the right side). The measurements were performed after the initial focus routine completed, and the expectation is thus to find a focus optimum near the center image in the sequence (reflecting a zero movement of the position of the detection objective). The objective position is shown together with the value of the DCTS focus metric above each image. An enlarged view of the region highlighted by the green box is shown in the bottom row. **b**, Dorsal view (xy) and anteroposterior view (yz) maximum-intensity projections of an image stack showing a late-stage *Drosophila* embryo (expressing a nuclear-localized fluorescent marker) after 21 h of AutoPilot-controlled time-lapse image acquisition. The recording started at the blastoderm stage. The locations of two of the reference planes used by the AutoPilot framework ( $z_0$  and  $z_4$ ) are indicated by red lines in the image to the right. **c**, Side-by-side comparison of image quality and spatial resolution in representative image regions for adaptively corrected (top row) and uncorrected (middle row) microscope states at the 21-h time point shown in **b**. The increase in spatial resolution (bottom row, green) was quantified by comparative analysis of the derivatives of intensity profiles crossing sharp edges in the image data, corresponding to boundaries of fluorescently labeled cell nuclei (bottom row). The computational procedure and its mathematical derivation are described in Royer et al.<sup>21</sup>. The data shown in **c** have been adapted with permission from Royer et al.<sup>21</sup>, Springer Nature Limited. Scale bars, 20  $\mu\text{m}$  (**a**, top; **b**); 5  $\mu\text{m}$  (**a**, bottom; **c**).

### Overview of the image and text logs of the AutoPilot framework

When using the AutoPilot framework for spatiotemporal adaptive imaging, the user has the option to save not only the primary image data of the experiment but also the images and text logs documenting the measurements, process workflow and decisions of the AutoPilot framework itself. These logs greatly simplify the task of verifying that performance of the AutoPilot framework is optimal and help the user identify potential problems with the initial setup of the framework or with the AutoPilot configuration used in a particular experiment. We included example log files from a multiview recording of *Drosophila* embryonic development as Supplementary Data 2.

Regarding the availability of image logs, the AutoPilot framework can be configured to store a series of defocus measurements (Fig. 7a) for each color channel, reference plane and relevant DOFs ( $D$  and  $Y$ ; as well as  $\alpha/\beta$ , if the user requests that these parameters be computed from defocus stacks; see Step 82).

Regarding the availability of text logs, the AutoPilot framework stores a variety of information in the following text files:

- ‘AF setup log.txt’. The autofocus (AF) setup log contains a record of the user-defined AutoPilot parameters in effect during the experiment.
- ‘AF state log.txt’. The AF state log contains the detection objective positions (columns D1, D2), light-sheet offsets (columns I1, I2), illumination objective positions (columns Y1, Y2),  $\alpha$  angles (columns A1, A2) and  $\beta$  angles (columns B1, B2) in use in each specimen (column SPEC), at each time point (column TP). The time points occurred at the indicated time (column TME) after the beginning of the recording. The values are shown for each laser wavelength in operation (column CLR) at each reference plane (column ZP). This log can be inspected to find sudden changes in values or changes in values that are larger than the user-defined search radius for each variable.
- ‘AF correction log.txt’. The AF correction log contains the corrections calculated for the parameters shown in the AF state log. The AF correction log shows these values as they were measured at the user-defined time-points (column TP).
- ‘AF debug log.txt’. The AF debug log contains an abbreviated version of the AF state log. For each specimen (column SPEC), time point (column TP), laser channel (column CH), reference plane (column ZP), camera (column CAM) and illumination arm (column ARM), the log shows the positions of the illumination objectives (columns P1, P3), the positions of the detection objectives (columns P2, P4), the light-sheet offsets (columns LS1, LS2) and the z-position of the sample stage (column Z). This log can be quickly scanned for unexpected changes in the microscope setup. For any given combination of reference plane, camera and illumination arm, the changes from one time point to the next should be gradual and within the user-defined search radii.
- ‘AF angles log.txt’. The AF angles log contains information about the  $\alpha$ - and  $\beta$ -angle measurements. For each specimen (column SPEC), time point (column TP), excitation wavelength (column CLR) and reference plane (column ZP), the log shows the raw  $\alpha$ - and  $\beta$ -angle measurements for light-sheet 1 (columns A1r, B1r), and the raw  $\alpha$ - and  $\beta$ -angle measurements for light-sheet 2 (columns A2r, B2r). These raw measurements are smoothed according to different schemes (median or none). Columns A1s, A2s, B1s and B2s contain the corresponding smoothed angles, and columns A1Med, A2Med, B1Med and B2Med show the results of median filtering across planes before and after sync planes.
- ‘AF Dcalc log.txt’. The AF Dcalc log contains the results of the stack\_analysis procedure described in Step 36, which measures the  $\alpha$  and  $\beta$  angles. For each specimen (column SPEC), time point (column TP), camera (column CAM), illumination arm (column ARM), excitation wavelength (column CLR) and reference plane (column ZP), the log shows the average of the dZ defocus measurements (column dZave), the average of the  $\alpha$ -angle measurements (column Aave) and the fit average of the  $\beta$ -angle measurements (column Bfit). The remaining entries (A, B and dZ) represent the raw measurement results.
- ‘AF Y log.txt’. The AF Y log contains values used to calculate the optimal position of the illumination objectives. For each specimen (column SPEC), time point (column TP), excitation wavelength (column CLR) and reference plane (column ZP), the log shows the raw Y measurements for light sheets 1 and 2 (columns Y1raw, Y2raw), and the respective parabola-smoothed values (columns Y1smth, Y2smth). Finally, the remaining columns (Y1a, Y1b and Y1c, as well as Y2a, Y2b and Y2c) contain the coefficients of the parabola fit ( $f(x) = ax^2 + bx + c$ ).
- ‘AF qpsolve log.txt’. The AF qpsolve log documents all function calls to the qpsolve function in the AutoPilot core library. Each block of five lines in the file corresponds to a single function call. All lines start with ‘SPECX’, where X is the specimen index, followed by ‘TPX’, where X is the time point index,

and by ‘Observ’, ‘Missing’, ‘Limits’, ‘Si’ or ‘Si + 1’. Lines containing ‘Observ’ correspond to the observation vector ( $D/I$  defocus measurements,  $\alpha$ -and  $\beta$ -angle measurements and Y measurements). Lines containing ‘Missing’ correspond to the Boolean vector specifying which measurements are missing. Lines containing ‘Limits’ correspond to the correction limits for each DOF. Lines containing ‘Si’ correspond to the current microscope state, and lines containing ‘Si + 1’ correspond to the new corrected microscope state returned by the function call to `qpsolve`.

### Use of AutoPilot log files for consistency checks and troubleshooting

Below, we will briefly discuss some useful consistency checks and the diagnosis of common problems based on these logs:

- One simple way to check whether the defocus correction was performed optimally is to inspect the image sequence (consisting of  $2n + 1$  images, where  $n$  is defined by the user) of a given defocus measurement. After focus optimization, the sharpest image should be the central image with index  $n + 1$ . The text log ‘AF state log.txt’ contains analogous information. A high-quality recording usually exhibits robust and smooth corrections, in both space and time.
- If the ‘Refocus Radius’ parameter (Fig. 6) is too small, the AutoPilot framework will lose accuracy in determining the perfect focus. A good focus curve (the set of focus values determined across the refocus range) should exhibit a full Gaussian-like profile; i.e., it should contain the global maximum as well as the two inflection points. Ideally, as a rule of thumb, the refocus radius should be roughly equal to the distance between the two inflection points of a representative defocus curve. Of course, the shape of focus curves is substantially influenced by the optical configuration of the microscope and to a lesser extent by the choice of sample, and parameter settings should be adjusted accordingly.
- Also important is the number of samples collected within the focus range  $[-r, +r]$ . If the number of samples is too small (the absolute minimum is 5) and the signal-to-noise ratio in the image data is low, the statistical tests performed by the AutoPilot library to verify the quality of a focus curve will be impaired. Typical settings for the number of samples are 5, 7 and 11. A larger number of samples will lead to a substantial increase in measurement/computation time and in the use of the specimen’s photon budget, and is therefore unadvisable unless absolutely necessary.
- A valid defocus curve can sometimes be rejected as invalid because the measurements are too noisy and have the statistical appearance of random observations. This rejection mechanism is useful for discarding bad data, e.g., when a reference plane is located outside of the sample. However, if valid defocus curves are incorrectly rejected, the ‘Min Fit Probability’ parameter may be set too high and must be lowered. Another possible solution is to increase the number of samples; however, this approach has some obvious disadvantages, as discussed in the point above. Note that lowering the ‘Min Fit Probability’ parameter substantially will eventually lead to the AutoPilot framework’s inability to detect low-quality focus curves and thus to occasional artifactual corrections when reference planes are located outside the sample or when image quality deep inside a sample precludes accurate focus measurements.
- If the movement direction of piezo positioners is flipped relative to the convention of the AutoPilot framework (as a result of an incompatible orientation of the piezo stage or operation of the control electronics), the corrections performed by the AutoPilot library will exhibit the wrong sign. In this case, instead of improving focus quality, the system will become increasingly misaligned after each AutoPilot iteration (approximately doubling the focus error in each step). To fix this issue, the user should first verify that the movement direction of the piezo positions is correct (see also the supplementary materials of Royer et al.<sup>21</sup>).
- Another common problem is that some sCMOS camera models exhibit higher background intensity levels on the first image of an acquisition sequence. This is detrimental to the side-by-side comparison of image quality across a series of image-based defocus measurements, in particular when working with weak signals owing to, e.g., low laser power settings or low fluorescent marker expression levels. In the SiMView control software, this problem is avoided by automatically discarding the first image in each image sequence. A similar strategy may be required when using the AutoPilot libraries in a different microscope control framework.

### Processing and analyzing light-sheet microscopy image datasets

Finally, we would like to note that most light-sheet microscopy datasets, in particular complex recordings involving the acquisition of multiple specimen views, require additional image-processing

software to convert the raw image data into a biologically meaningful representation and/or into a fused or multiview deconvolved version of the image data. Several software solutions that help with these essential image processing and data analysis steps are readily available and complement the methods described in this protocol. A few examples of useful tools that have been tested extensively on large-scale light-sheet microscopy datasets are listed below.

- Multiview registration, content-based fusion and deconvolution: Preibisch et al.<sup>44,45</sup>, Chhetri et al.<sup>17</sup> and Amat et al.<sup>23</sup>
- Cell segmentation and cell tracking based on nuclear markers: Amat et al.<sup>10</sup>
- Cell shape segmentation based on membrane markers: Stegmaier et al.<sup>25</sup>
- Large-scale image data management and image compression: Amat et al.<sup>23</sup> and Balazs et al.<sup>46</sup>
- Analysis of functional image data: Freeman et al.<sup>47</sup> and Lemon et al.<sup>16</sup>
- Interactive visualization and annotation of multiview image data: Wolff et al.<sup>22</sup>

## References

1. Winter, P. W. & Shroff, H. Faster fluorescence microscopy: advances in high speed biological imaging. *Curr. Opin. Chem. Biol.* **20**, 46–53 (2014).
2. Power, R. M. & Huisken, J. A guide to light-sheet fluorescence microscopy for multiscale imaging. *Nat. Methods* **14**, 360–373 (2017).
3. Stelzer, E. H. Light-sheet fluorescence microscopy for quantitative biology. *Nat. Methods* **12**, 23–26 (2014).
4. Keller, P. J. & Ahrens, M. B. Visualizing whole-brain activity and development at the single-cell level using light-sheet microscopy. *Neuron* **85**, 462–483 (2015).
5. Keller, P. J., Schmidt, A. D., Wittbrodt, J. & Stelzer, E. H. K. Reconstruction of zebrafish early embryonic development by scanned light sheet microscopy. *Science* **322**, 1065–1069 (2008).
6. Keller, P. J. et al. Fast, high-contrast imaging of animal development with scanned light sheet-based structured-illumination microscopy. *Nat. Methods* **7**, 637–642 (2010).
7. Tomer, R., Khairy, K., Amat, F. & Keller, P. J. Quantitative high-speed imaging of entire developing embryos with simultaneous multiview light-sheet microscopy. *Nat. Methods* **9**, 755–763 (2012).
8. Krzic, U., Gunther, S., Saunders, T. E., Streichan, S. J. & Hufnagel, L. Multiview light-sheet microscope for rapid *in toto* imaging. *Nat. Methods* **9**, 730–733 (2012).
9. Schmid, B. et al. High-speed panoramic light-sheet microscopy reveals global endodermal cell dynamics. *Nat. Commun.* **4**, 2207 (2013).
10. Amat, F. et al. Fast, accurate reconstruction of cell lineages from large-scale fluorescence microscopy data. *Nat. Methods* **11**, 951–958 (2014).
11. Wu, Y. et al. Inverted selective plane illumination microscopy (iSPIM) enables coupled cell identity lineage and neurodevelopmental imaging in *Caenorhabditis elegans*. *Proc. Natl. Acad. Sci. USA* **108**, 17708–17713 (2011).
12. Wu, Y. et al. Spatially isotropic four-dimensional imaging with dual-view plane illumination microscopy. *Nat. Biotechnol.* **31**, 1032–1038 (2013).
13. Panier, T. et al. Fast functional imaging of multiple brain regions in intact zebrafish larvae using selective plane illumination microscopy. *Front. Neural Circuits* **7**, 65 (2013).
14. Ahrens, M. B. & Keller, P. J. Whole-brain functional imaging at cellular resolution using light-sheet microscopy. *Nat. Methods* **10**, 413–420 (2013).
15. Wolf, S. et al. Whole-brain functional imaging with two-photon light-sheet microscopy. *Nat. Methods* **12**, 379–380 (2015).
16. Lemon, W. C. et al. Whole-central nervous system functional imaging in larval *Drosophila*. *Nat. Commun.* **6**, 7924 (2015).
17. Chhetri, R. K. et al. Whole-animal functional and developmental imaging with isotropic spatial resolution. *Nat. Methods* **12**, 1171–1178 (2015).
18. Voie, A. H., Burns, D. H. & Spelman, F. A. Orthogonal-plane fluorescence optical sectioning: three-dimensional imaging of macroscopic biological specimens. *J. Microsc.* **170**, 229–236 (1993).
19. Fuchs, E., Jaffe, J., Long, R. & Azam, F. Thin laser light sheet microscope for microbial oceanography. *Opt. Express* **10**, 145–154 (2002).
20. Huisken, J., Swoger, J., Del Bene, F., Wittbrodt, J. & Stelzer, E. H. K. Optical sectioning deep inside live embryos by selective plane illumination microscopy. *Science* **305**, 1007–1009 (2004).
21. Royer, L. A. et al. Adaptive light-sheet microscopy for long-term, high-resolution imaging in living organisms. *Nat. Biotechnol.* **34**, 1267–1278 (2016).
22. Wolff, C. et al. Multi-view light-sheet imaging and tracking with the MaMuT software reveals the cell lineage of a direct developing arthropod limb. *Elife* **7**, e34410 (2018).
23. Amat, F. et al. Efficient processing and analysis of large-scale light-sheet microscopy data. *Nat. Protoc.* **10**, 1679–1696 (2015).
24. Khairy, K., Lemon, W., Amat, F. & Keller, P. J. A preferred curvature-based continuum mechanics framework for modeling embryogenesis. *Biophys. J.* **114**, 267–277 (2018).

25. Stegmaier, J. et al. Real-time three-dimensional cell segmentation in large-scale microscopy data of developing embryos. *Dev. Cell* **36**, 225–240 (2016).
26. Grimm, J. B. et al. A general method to fine-tune fluorophores for live-cell and in vivo imaging. *Nat. Methods* **14**, 987–994 (2017).
27. Liu, Z. & Keller, P. J. Emerging imaging and genomic tools for developmental systems biology. *Dev. Cell* **36**, 597–610 (2016).
28. Keller, P. J. Imaging morphogenesis: technological advances and biological insights. *Science* **340**, 1234168 (2013).
29. Liu, T. L. et al. Observing the cell in its native state: imaging subcellular dynamics in multicellular organisms. *Science* **360**, 6386 (2018).
30. Baumgart, E. & Kubitscheck, U. Scanned light sheet microscopy with confocal slit detection. *Opt. Express* **20**, 21805–21814 (2012).
31. Fahrbach, F. O. & Rohrbach, A. Propagation stability of self-reconstructing Bessel beams enables contrast-enhanced imaging in thick media. *Nat. Commun.* **3**, 632 (2012).
32. de Medeiros, G. et al. Confocal multiview light-sheet microscopy. *Nat. Commun.* **6**, 8881 (2015).
33. Silvestri, L., Bria, A., Sacconi, L., Iannello, G. & Pavone, F. S. Confocal light sheet microscopy: micron-scale neuroanatomy of the entire mouse brain. *Opt. Express* **20**, 20582–20598 (2012).
34. Rohrbach, A. Artifacts resulting from imaging in scattering media: a theoretical prediction. *Opt. Lett.* **34**, 3041–3043 (2009).
35. Huisken, J. & Stainier, D. Y. Even fluorescence excitation by multidirectional selective plane illumination microscopy (mSPIM). *Opt. Lett.* **32**, 2608–2610 (2007).
36. Truong, T. V., Supatto, W., Koos, D. S., Choi, J. M. & Fraser, S. E. Deep and fast live imaging with two-photon scanned light-sheet microscopy. *Nat. Methods* **8**, 757–760 (2011).
37. Planchon, T. A. et al. Rapid three-dimensional isotropic imaging of living cells using Bessel beam plane illumination. *Nat. Methods* **8**, 417–423 (2011).
38. Fahrbach, F. O., Simon, P. & Rohrbach, A. Microscopy with self-reconstructing beams. *Nat. Photonics* **4**, 780–785 (2010).
39. Chen, B. C. et al. Lattice light-sheet microscopy: imaging molecules to embryos at high spatiotemporal resolution. *Science* **346**, 1257998 (2014).
40. Dunsby, C. Optically sectioned imaging by oblique plane microscopy. *Opt. Express* **16**, 20306–20316 (2008).
41. Bouchard, M. B. et al. Swept confocally-aligned planar excitation (SCAPE) microscopy for high speed volumetric imaging of behaving organisms. *Nat. Photonics* **9**, 113–119 (2015).
42. Palero, J., Santos, S. I., Artigas, D. & Loza-Alvarez, P. A simple scanless two-photon fluorescence microscope using selective plane illumination. *Opt. Express* **18**, 8491–8498 (2010).
43. Keller, P. J., Pampaloni, F. & Stelzer, E. H. Three-dimensional preparation and imaging reveal intrinsic microtubule properties. *Nat. Methods* **4**, 843–846 (2007).
44. Preibisch, S., Saalfeld, S., Schindelin, J. & Tomancak, P. Software for bead-based registration of selective plane illumination microscopy data. *Nat. Methods* **7**, 418–419 (2010).
45. Preibisch, S. et al. Efficient Bayesian-based multiview deconvolution. *Nat. Methods* **11**, 645–648 (2014).
46. Balazs, B., Deschamps, J., Albert, M., Ries, J. & Hufnagel, L. A real-time compression library for microscopy images. Preprint at *bioRxiv*, <https://doi.org/10.1101/164624> (2017).
47. Freeman, J. et al. Mapping brain activity at scale with cluster computing. *Nat. Methods* **11**, 941–950 (2014).

### Acknowledgements

We thank all members of the Keller Lab for extensive testing of the AutoPilot framework and for their contributions to the development of this method, M. Coleman (Coleman Technologies) for custom microscope operating software, B. Coop and the jET team at the Janelia Research Campus for mechanical designs and custom mechanical parts, and M. Staley for help with producing the video demonstrating the specimen-embedding procedure. This work was supported by the Howard Hughes Medical Institute and the Chan Zuckerberg Biohub.

### Author contributions

All authors contributed to the development of the protocol and the writing of the manuscript.

### Competing interests

P.J.K., R.K.C. and L.A.R. filed provisional US patent application 62,354,384 for adaptive light-sheet microscopy on 24 June 2016. P.J.K. holds US patent 9,404,869 for simultaneous multiview light-sheet microscopy, issued 2 August 2016.

### Additional information

Supplementary information is available for this paper at <https://doi.org/10.1038/s41596-018-0043-4>.

Reprints and permissions information is available at [www.nature.com/reprints](http://www.nature.com/reprints).

Correspondence and requests for materials should be addressed to L.A.R. or P.J.K.

Publisher's note: Springer Nature remains neutral with regard to jurisdictional claims in published maps and institutional affiliations.

Published online: 26 October 2018

**Related links**

**Key references using this protocol**

- Royer, L. A. et al. *Nat. Biotechnol.* **34**, 1267–1278 (2016): <https://doi.org/10.1038/nbt.3708>  
Amat, F. et. al. *Nat. Methods* **11**, 951–958 (2014): <https://doi.org/10.1038/nmeth.3036>  
Stegmaier, J. et al. *Dev. Cell* **36**, 225–240 (2016): <https://doi.org/10.1016/j.devcel.2015.12.028>  
Grimm, J. B. et al. *Nat. Methods* **14**, 987–994 (2017): <https://doi.org/10.1038/nmeth.4403>